Rowland, G. H., Ng, H. C., Robinson, L. F., McManus, J. F., Mohamed, K. J., & McGee, D. (2017). Investigating the use of $^{232}Th/^{230}Th$ as a dust proxy using co-located seawater and sediment samples from the low-latitude North Atlantic. *Geochimica et Cosmochimica Acta*, *214*, 143-156. https://doi.org/10.1016/j.gca.2017.07.033

Peer reviewed version

Link to published version (if available):
10.1016/j.gca.2017.07.033

Link to publication record in Explore Bristol Research
PDF-document

This is the accepted author manuscript (AAM). The final published version (version of record) is available online via Elsevier at DOI: 10.1016/j.gca.2017.07.033. Please refer to any applicable terms of use of the publisher.

Investigating the use of $^{232}Th/^{230}Th$ as a dust proxy using co-located seawater and sediment samples from the low-latitude North Atlantic

George H. Rowland [a*] Hong Chin Ng [a] Laura F. Robinson [a] Jerry F. McManus [b] Kais J. Mohamed [c] David McGee [d]

[a]School of Earth Sciences,Wills Memorial Building, University of Bristol, Bristol, BS8 1RJ, UK (*correspondence: gr1850@bristol.ac.uk)

[b] Lamont-Doherty Earth Observatory of Columbia University, 61 Route 9W, Palisades, New York 10964, USA

[c] Departmento Geociencias Marinas y Ordenación del Territorio, Facultad de Ciencias del Mar, Universidad de Vigo, 36310 Vigo

[d] Massachusetts Institute of Technology, 45 Carleton Street, Building E25, Room 625, Cambridge, MA 02142

Abstract

The thorium isotope ratio $^{232}Th/^{230}Th$ can be measured in seawater and sediment samples, and has been used as a proxy to reconstruct lithogenic fluxes to the oceans for the modern day and the Pleistocene. There has not yet been a study testing the proxy using the $^{232}Th/^{230}Th$ ratio in seawater and the ratio recorded in the underlying sediment. In this study we use co-located core-top sediments and seawater samples from five seamount sites spanning the tropical North Atlantic to investigate the link between seawater and sediment $^{232}Th/^{230}Th$ ratios across a range of water depths. Our results indicate that a broad correlation exists between seawater and sedimentary $^{232}Th/^{230}Th$ ratios. Both seawater and sedimentary $^{232}Th/^{230}Th$ ratios record a signal consistent with decreasing lithogenic input east to west, from Africa to South America. However, calculated ^{232}Th fluxes for the core-top sediment samples indicate a strong dependence on depth, with up to a factor of ~4 difference from shallow (<600 m) to deep sites (>2900 m). This depth dependence is likely caused by either a deficit of ^{230}Th burial at depth compared to the production in the overlying water column, through addition of ^{232}Th, or by a combination of the two processes. By comparing seawater and sedimentary $^{232}Th/^{230}Th$ ratios we derive an apparent fractional solubility of ^{232}Th of 29 ± 3%, in reasonable agreement with the upper end of existing estimates.

1. Introduction

Aeolian dust is an important but poorly quantified part of the climate system. Dust affects the climate through interaction with radiation in the Earth's atmosphere and plays a part in the carbon cycle by delivering key micronutrients, such as iron, to the ocean (Jickells et al., 2005; Maher et al., 2010). Knowledge of present day dust fluxes to the ocean comes from model simulations (Mahowald et al., 2005), direct observations (Lawrence and Neff, 2009) and geochemical data (Measures et al., 2008; Hsieh et al., 2011). Model simulations provide a global picture of dust fluxes to the oceans (Niedermeier et al., 2014), but rely on poorly constrained parameters such as the surface properties of the dust source regions, giving rise to uncertainties in simulated fluxes (Mahowald et al., 2005). Given the relative scarcity of direct observations (Kohfeld and Harrison, 2001), geochemical proxy methods provide a means of testing and improving these models as well as our knowledge of dust fluxes (Anderson et al., 2016).

A widely used method has been the measurement of Al concentrations in the dissolved phase in seawater e.g. (Measures et al., 2008). This approach draws on the fact that the main supply of Al to the ocean is from continentally-derived lithogenic particles. In remote parts of the ocean, dust is the main source of continental material, and so dissolution of these grains leads to a measurable dissolved Al concentration that is correlated with expected dust input (Hydes, 1983). However, a key difficulty in using dissolved Al to reconstruct dust fluxes is in calculating a local residence time (Hsieh et al., 2011). A related geochemical method that allows for the calculation of a local residence time is the combined measurement of two isotopes of thorium: ^{232}Th and ^{230}Th (Hsieh et al., 2011; Hayes et al., 2013).

Th-232 is a long lived (half-life = 1.4×10^{10} yrs; Holden, 1990) primordial nuclide that is found in the upper continental crust at a concentration of approximately 11 ppm (Taylor and McLennan, 1985). As for Al, ^{232}Th is concentrated in the continental crust, so it can be used to trace lithogenic material with a continental origin. Dissolved ^{232}Th in seawater is therefore assumed to be derived from the dissolution of continental detritus in seawater (Hsieh et al., 2011; Hayes et al., 2013; Deng et al., 2014; Lopez et al., 2015). Given that ^{232}Th provides a means of tracking the input of continental material to the ocean, the only other factor needed in order to calculate a flux of dust is a timescale for ^{232}Th addition. The shorter lived isotope ^{230}Th can be used to provide this timescale. Th-230 has a half life of 75,584 yrs (Cheng et al., 2013), and is sourced from the radioactive decay of ^{234}U in seawater. Th-230 is scavenged rapidly onto sediment particles (although the adsorbed ^{230}Th is thought to maintain a reversible exchange with a pool of dissolved ^{230}Th; Bacon and Anderson, 1982),

meaning that ^{230}Th has a short oceanic residence time of up to ~40 yrs (Anderson et al., 1983). The residence time of ^{230}Th in seawater can be derived from measurements of ^{230}Th activity in seawater combined with the known production of ^{230}Th from ^{234}U (Broecker et al., 1973). Making the assumption that ^{230}Th and ^{232}Th share the same residence time, the seawater dissolved ^{232}Th concentration can be combined with the ^{230}Th-derived residence time, to determine a flux of dissolved ^{232}Th. Combining dissolved flux estimates with estimates of the fractional solubility of ^{232}Th from continental material allows a total flux of ^{232}Th to be estimated (Hsieh et al., 2011; Hayes et al., 2013; Deng et al., 2014). Estimates of solubility currently account for a significant source of uncertainty in studies that estimate total ^{232}Th flux from dissolved ^{232}Th fluxes (Hsieh et al., 2011; Hayes et al., 2013).

Both these isotopes of thorium have also been measured in sediments in order to estimate lithogenic fluxes in the past (Pourmand et al., 2004; Anderson et al., 2006; McGee et al., 2007; Winckler et al., 2008; Lam et al., 2013; Serno et al., 2014; Costa et al., 2016; Jacobel et al., 2016; Kienast et al., 2016; Williams et al., 2016). In this scenario ^{232}Th measured in sediments is assumed to be sourced only from the input of continental detritus (Pourmand et al., 2004; Anderson et al., 2006; McGee et al., 2007). Far from ocean margins it has been assumed that all ^{232}Th in the sediment (in both adsorbed and lattice-bound pools) is sourced from continental aeolian dust (Anderson et al., 2006; McGee et al., 2007; Hsieh et al., 2011; Hayes et al., 2013; Lopez et al., 2015).

The two thorium based methods described above both make use of the constant input of the isotope ^{230}Th in order to calculate a timescale. The intense scavenging from the water column leads to efficient removal of ^{230}Th. If the flux of ^{230}Th to the sediment is assumed to be equal to the production flux of ^{230}Th in the overlying water column (β, ~0.0267 dpm m^{-3} yr^{-1}; Francois et al., 2004), then the $^{230}Th_{xs}$ activity concentration (in dpm g^{-1}, where 'xs' denotes excess ^{230}Th that is not supported by ^{234}U decay in the sediment) in the sediment is a function of the sediment flux to the seafloor. Therefore measurement of $^{230}Th_{xs}$ in the sediment allows vertical mass fluxes at a given water depth (z, in metres) to be calculated (Equation 1). This method of calculating vertical sediment fluxes is termed '^{230}Th normalisation' (Francois et al., 2004). Early studies used this method to calculate lithogenic fluxes in the Atlantic (Francois and Bacon, 1991). By combining the sediment mass flux calculated by ^{230}Th normalisation with the fractional concentration of ^{232}Th in the sediment (in μg g^{-1}), a vertical flux of ^{232}Th (in μg m^{-2} yr^{-1}) to the seafloor can be calculated (Equation 2). If the ^{232}Th concentration in lithogenic material is known, then an estimate of the lithogenic flux can be made (e.g. McGee et al., 2007). Recently it has been suggested that a concentration of 14 ppm is appropriate for estimating dust fluxes using this method for most locations

receiving fine-grained dust (McGee et al., 2016). If the $^{232}Th/^{230}Th$ ratio of the adsorbed phase of thorium is known ($(^{232}Th/^{230}Th_{xs})_{Ads}$ in μg dpm^{-1}), an adsorbed flux of ^{232}Th can also be calculated (Robinson et al., 2008; Equation 3). This 'adsorbed' pool of thorium can be accessed by leaching sediments without dissolving the ^{232}Th bearing lithogenic phases (Robinson et al., 2008).

Equation 1. Sedimentary mass flux = $\beta * z / {}^{230}Th_{xs}$

Equation 2. ^{232}Th flux = Sedimentary mass flux * ^{232}Th

Equation 3. Adsorbed ^{232}Th flux = $(^{232}Th/^{230}Th_{xs})_{Ads} * \beta * z$

Determination of ^{232}Th and ^{230}Th in ocean sediments and seawater therefore has the potential to provide the basis for estimating fluxes of continental material (both in the past and in modern times). However, there has not yet been a study that combines measurements of ^{232}Th and ^{230}Th in core-top sediments with co-located seawater samples.

In this study, we assess the relationship between modern seawater and core-top sedimentary $^{232}Th/^{230}Th$ ratios in the tropical North Atlantic Ocean. This area is, in part, beneath the path of dust emitted from the largest dust source on Earth, the Sahara Desert (Goudie and Middleton, 2001; Cakmur et al., 2006). We present measured $^{232}Th/^{230}Th$ ratios and concentrations in core-top sediments and seawater samples, and compare how the values vary across the basin as well as with water depth. We calculate ^{230}Th-normalised mass fluxes and ^{232}Th fluxes for our sample sites and investigate the spatial and vertical variability of these parameters. We also estimate the apparent fractional solubility of ^{232}Th, a parameter that is poorly constrained but essential for calculating total fluxes of ^{232}Th from dissolved ^{232}Th concentrations in seawater (Hsieh et al., 2011).

2. Study area, sampling strategy and sample collection

Core-top sediments were collected from five sites from the JC094 TROPICS (TRacing Oceanic Processes usIng Corals and Sediments) cruise aboard RRS *James Cook* during October and November 2013 (Figure 1; Robinson, 2014). The sampling strategy exploited extremes in bathymetry to provide core-top sediment samples from 570 m to 4565 m. The five sampling locations are named based on their proximity to major bathymetric features (Figure 1). The 'Carter' and 'Knipovich' sites are seamounts in the eastern basin, 'Vema' makes up part of the Vema fracture zone on the mid-Atlantic ridge, whilst 'Vayda' and 'Gramberg' are two seamounts from the Researchers Seamounts in the western basin. The

targeting of bathymetric highs spanning the Atlantic allows approximate sedimentary depth transects to be constructed at each location.

Short mega-core and remotely operated vehicle (ROV) push-core sampling equipment were used in order to ensure the best possible preservation of sediment core-tops. In one instance box-core apparatus was used to collect a core-top sample. Core samples were stored at 5^{o}C. Radiocarbon ages for all core-top sediments (derived from planktonic foraminifera) indicate that they are between 1000 and 8870 yr BP, with an average age of ~4300 yr BP (supplementary information).

Seawater samples (~5 L) were collected close to the core-top sample sites by Niskin bottles on the CTD rosette, the ROV, or mounted on the mega-core frame and were filtered through acropak (0.2 µm) filters into acid-cleaned plastic jerry cans, and acidified on the day of collection with 5ml of concentrated ultrapure hydrochloric acid.

3. Analytical procedures

3.1 Sediment dissolution laboratory procedure

Aliquots of dried sediment (~0.5 g) were taken from the top 1 cm of each core and then mechanically homogenised using an agate mortar and pestle. Approximately 0.1 g aliquots of the homogenised sediment were weighed out and spiked with a mixed ^{236}U and ^{229}Th spike. The samples were dissolved in 7 ml 14 N HNO_3, 3 ml 28 N HF and 2 ml 11.6 N $HClO_4$. The samples were passed through columns containing 1.5 ml of an anion exchange resin (Eichrom 1-X8 100-200 mesh) in order to separate U and Th. The Th fraction was further purified through a second anion exchange column. Th separates were refluxed with $HClO_4$ and H_2O_2 to eliminate organic matter, and the U separates were refluxed with H_2O_2 only. Two procedural blanks were analysed with each batch of 8 samples.

3.2 Sediment leaching laboratory procedure

The method used broadly followed that of Robinson et al. (2008). Approximately 0.1 g of homogenised sediment (from the same aliquots used in the total dissolution procedure) from the Carter Seamount samples were leached in 3 N HCl for 20 minutes with ultrasonication. The samples were then centrifuged, and the supernatant liquid was pipetted from the centrifuge tubes. The supernatant liquid was then weighed and spiked with both ^{236}U and ^{229}Th spikes. The samples were then passed through anion exchange resin as for the total dissolution procedure.

3.3 Seawater analysis

Seawater samples were spiked with ^{229}Th and ^{236}U and allowed to equilibrate before being precipitated with ammonium hydroxide to a pH of 7.5-8. The supernatant was removed using a peristaltic pump, and the precipitate dissolved in concentrated hydrochloric acid, before separation of Th and U isotopes using anion exchange column chromatography. The methods for the separation of Th and U isotopes follow those set out by Auro et al. (2012).

3.4 Mass spectrometric analysis

Mass spectrometry was carried out using a Thermo Scientific Neptune multi-collector inductively coupled plasma mass spectrometer (MC-ICP-MS; Auro et al., 2012; Chen et al., 2015). A standard bracketing method was used in order to apply corrections for mass bias and ion counter yield; in-house thorium (Th-SGS) and the uranium standards U-112a were used as bracketing standards. Sample uptake was through a CETAC Aridus desolvating nebulizer. Measurement at half masses (230.5, 229.5, 228.5) accounted for the tailing effect of ^{232}Th. The same procedure was applied to U measurements at half masses 234.5 and 233.5 to account for ^{238}U tailing. An exponential tail profile was assumed for interpolation between half masses (Hoffman et al., 2007). The size of the ^{232}Th tailing correction on the ^{230}Th beam was <2% of the ^{230}Th beam for nearly all samples (abundance sensitivity of ~0.5 ppm of the ^{232}Th beam intensity at mass 230). The average sizes of full procedural blanks from three separate batches of total dissolution of sediment analyses (with approximate fractional size of blanks compared to the sample signal shown in parentheses) are: 29 ± 6.3 pg ^{232}Th (~0.015 %), 4.3 ± 1.5 fg ^{230}Th (~0.054 %), 70 ± 120 pg ^{238}U (~<0.5 %), 42 ± 7.0 fg ^{234}U (~1.3 %), (uncertainties are given as 2 standard errors from the mean). The uncertainty of the ^{238}U blank reflects the fact that one analysis had a much higher blank than the other two (but still <0.5% of sample signals).

Procedural blanks from the leaching procedure are 2.4 ± 0.63 pg ^{232}Th (~0.024%), 0.01 ± 0.027 fg ^{230}Th (~0.004%), and U blanks were negligible. The average procedural blanks from two separate seawater procedures are 6.8 ± 2.4 pg ^{232}Th (~1-5%, except for two samples with lower ^{232}Th concentration which are ~10%) and 0.6 ± 0.5 fg ^{230}Th (~0.2-4%).

3.5 Carbonate content determination

Carbonate contents of the sediments were determined using a Carlo Erba NC2500 elemental analyser at the University of Liverpool. Small aliquots of sediment were analysed for total carbon, exposed to HCl fumes overnight in order to digest the carbonate fraction, and were then analysed for organic carbon. The carbonate content of the sediment was calculated from the difference between the total carbon and organic carbon. The aliquots of

sediment were run in duplicate, with the average uncertainty of all 18 samples ~ ± 0.5% (based on 2 standard deviations from the mean; supplementary information).

3.6 Opal content determination

Biogenic opal analysis was carried out at the University of Bristol broadly following the procedures of Mortlock and Froelich (1989). About 50 mg of mechanically homogenised dry sediment was exposed to 5 ml of 1 N HCl and 5 ml of 10% H_2O_2 and agitated in an ultrasonic bath to remove carbonates and organics. Samples were centrifuged in deionised water, and the supernatants removed before drying of the residual sediment in an oven. The biogenic opal fraction was leached from the dry sediment by adding 40 ml 2 M Na_2CO_3 and heating in a water bath at 80ºC for 5 hours. Duplicates of each sample were prepared by pipetting off two separate aliquots from the supernatant. Opal contents were determined using a Hach DR3900 spectrophotometer following the molybdate-blue spectrophotometry procedures and reagents recommended by the Hach Company. Prior to sample analysis, instrumental baseline was determined and internally corrected for by measuring a blank.

4. Results

4.1 Filtered seawater ^{232}Th and ^{230}Th

Th-230 concentrations range from 4 to 15 fg kg^{-1} (Figure 2a; supplementary information) in good agreement with previously reported nearby data (Moran et al., 2002). Above ~2500 m depth at Carter, Knipvoch and Vema, seawater ^{230}Th concentrations show an approximately linear increase with depth, but below ~2500 m the rate of concentration increase at Carter and Knipovich profiles decreases (Figure 2a). Th-230 concentrations from Vayda do not show any obvious trend with depth (Figure 2a). Th-232 concentrations from all sites are in broad agreement with previous measurements at nearby stations (Moran et al., 2002). Th-232 concentrations do not show any obvious overall trends with depth and range from 14 to 97 pg kg^{-1} (Figure 2b; supplementary information). Seawater $^{232}Th/^{230}Th$ atom ratios range from 3400 to 14500 (Figure 3; supplementary information), also in broad agreement with previously reported $^{232}Th/^{230}Th$ ratios from nearby stations (Moran et al., 2002). In general, ratios decrease with depth and are higher at eastern sites compared to western sites across the range of depths sampled (Figure 3).

4.2 Core-top sediment ^{232}Th and ^{230}Th

Sedimentary $^{230}Th_{xs}$ concentrations increase with depth at all seamounts with a range of 1.1 to 12.6 dpm g^{-1}. Vayda seamount (in the West) shows the highest values at depth, whilst the concentrations across all stations converge at shallower depths (Figure 2c).

Th-232 concentrations in core-top sediments range from 0.80 to 5.9 μg g^{-1} and increase with depth at all seamount locations (Figure 2d). The magnitude of ^{232}Th concentration change with depth is a factor of 5 at the Carter seamount (in the East). The trends in ^{232}Th and $^{230}Th_{xs}$ concentration with depth above about 3000 m are close to linear, but below 3000 m the rate of concentration change increases.

Total sediment digest $^{232}Th/^{230}Th_{xs}$ atom ratios for all seamounts range from 13,000 to 43,000 (Figure 3). At all locations the ratios show an overall decrease from the shallowest to deepest sample sites. However, there is variation at intermediate depths notably at Carter and Vema which show a mid-depth minimum and a mid-depth maximum respectively. Generally, ratios are lower in the West and higher in the East.

Leached core-top sediment $^{232}Th/^{230}Th$ atomic ratios generally decrease with depth, with a range of 8600 to 25700 (Figure 3). The leached ($^{234}U/^{238}U$) activity ratios (supplementary information) are close to the seawater value of 1.147 (Robinson et al., 2004).

4.3 Carbonate and opal contents

The carbonate content ranges from 58-90 %. The carbonate content typically decreases with depth, and the rate of carbonate change with depth increases at depths >3000 m (Figure 4a).

The opal content of the sediment ranges from 0.6-3.4 %. The Opal content of the sediments increase with depth and show a strong negative correlation with carbonate content (R^2=0.91; supplementary information).

4.4 ^{230}Th-normalised sedimentary fluxes

Calculated mass fluxes range from 8 to 22 g m^{-2} yr^{-1} (Figure 4b). Mass fluxes are variable down to 2000 m, and at greater depths mass fluxes then decrease with depth. There is a broad trend of decreasing maximum mass flux from eastern to western sites.

Calculated ^{232}Th fluxes range from 9 to 63 μg m^{-2} yr^{-1} (Figure 4c). An increase in ^{232}Th flux with depth is seen at each sample site, ranging in magnitude from a factor of ~4.3 at Vema to a factor of ~1.2 at Gramberg. The increase at Carter Seamount is factor of ~3.6 over the entire depth transect, and ~1.4 between 2719 and 4565 m. At depths >~2000 m a broad trend in ^{232}Th fluxes can be seen between sample locations, with higher fluxes in the east (e.g. Carter and Knipovich) and lower fluxes in the west (Vayda and Gramberg; Figure 4c).

Calculated ^{232}Th fluxes from the leached Carter sediment range from 9 to 23 μg m^{-2} yr^{-1}. There is a general trend, approximately doubling with depth, that correlates strongly with total ^{232}Th fluxes from Carter (R^2 =0.99).

5. Discussion

5.1 ^{232}Th and ^{230}Th in seawater and sediment

The new seawater and sedimentary Th concentration profiles and ^{232}Th/^{230}Th ratios are generally in line with expectations, based on the findings of previous studies (Moran et al., 2002; Robinson et al., 2008; Hsieh et al., 2011; Deng et al., 2014). At four sites the ^{230}Th in seawater increases with depth, consistent with reversible scavenging (Bacon and Anderson, 1982). The departure from linear increases in ^{230}Th concentration below ~2500 m recorded at Carter, Knipovich and Vema is consistent with previous observations in the Atlantic (Marchal et al., 2007). This feature may be explained by ventilation of deep waters (Moran et al., 2002; Marchal; et al., 2007; Hayes et al., 2015a), enhanced scavenging in deep waters due to a bottom scavenging effect (Okubo et al., 2012), or potentially by vertical variations in the rates of adsorption versus desorption (Lerner et al., 2016). An exception to this typical profile is seen at Vayda, where the ^{230}Th (and ^{232}Th) concentration in seawater decreases at mid-depth. Given the deviation from the expected profiles of both isotopes and the location of the Vayda site relatively close to the mid-Atlantic ridge, the presence of a hydrothermal plume could offer an explanation for the trends seen at this site. This interpretation is supported by previous studies demonstrating the likelihood of a number of undiscovered hydrothermal vents on the ridge (Beaulieu et al., 2015) and that hydrothermal plumes strongly scavenge thorium in the North Atlantic (Hayes et al., 2015b). The profiles of ^{232}Th in seawater are broadly consistent with a surface source of ^{232}Th (i.e. dust) followed by a reversible scavenging behaviour. The exact profile would depend on the relative rates of particle sinking, adsorption and desorption (Lerner et al., 2016), but we observed profiles with no clear vertical trends. The ^{232}Th/^{230}Th ratios generally decrease with depth in all phases (seawater, total digestions of sediments and sediment leachates), as expected from in-situ production and subsequent reversible scavenging behaviour of ^{230}Th and the approximately constant vertical profiles of ^{232}Th.

Leaching of sediments can help to constrain the adsorbed pool of thorium bound to sediment surfaces. The ratio of adsorbed ^{232}Th/^{230}Th is expected to be the same as that of the dissolved thorium in the water column (Robinson et al., 2008). The ^{232}Th/^{230}Th ratios of leached sediment samples from Carter show a positive correlation with co-located seawater samples (R^2= 0.81), but with systematically slightly higher values (Figure 3). However, the leached ^{232}Th/^{230}Th ratios correlate even more strongly with those of the total sediment

digestions (R^2=0.86). This correlation along with the elevation of the leachate ratios (relative to the seawater ratios) are most simply explained by release of some lattice bound ^{232}Th that is accessed by the leaching procedure. Although Robinson et al. (2008) showed little change in ^{232}Th/^{230}Th when leaching in HCl ranging in concentration from 0.1-6 N, the liberation of extra ^{232}Th by 3 N HCl does provide a plausible explanation for the elevated leached ratios presented here.

5.2 ^{230}Th-normalised flux trends with location

Mass fluxes at depths ~500-2000 m do not show any coherent spatial trends, however for samples at depths below ~2000 m there is a broad pattern of higher ^{230}Th-normalised mass fluxes in the east compared to the west (Figure 4b). Although subtle, this gradient is consistent with higher biological productivity in the east (as indicated by chlorophyll concentrations in surface waters, Wang et al., 2013).

Continental material to the low latitude Atlantic is expected to be supplied from Saharan dust (Ridley et al., 2012), with higher continental inputs generally expected at sites in the east (e.g. Mahowald et al., 2005). Indeed, increasing seawater ^{232}Th/^{230}Th ratios at sites underlying the Saharan dust plume have previously been identified from a latitudinal transect at approximately 30^{o}W (Hsieh et al., 2011). With scavenging of all of the ^{230}Th produced in-situ to the sediment we would expect the ^{232}Th/^{230}Th ratios (and ^{232}Th fluxes) to be higher in the east than the west. As with the ^{230}Th-normalised mass fluxes, we do observe a broad east to west trend in maximum ^{232}Th fluxes (Figure 4c). At our sites, seasonal variations in dust deposition may also play a role in controlling the spatial patterns of dust flux recorded. For example, Carter and Knipovich lie under the approximate latitude of the winter dust plume, whereas Vayda and Gramberg (further north) lie in the range of summer dust and Vema could receive dust from both summer and winter dust plumes (Eglinton et al., 2002). In addition, it is possible that sites close to the basin margins may receive some direct contribution of lithogenic material from the continents (Francois and Bacon, 1991). However, even with these potential complications, we do see an overall decrease in ^{232}Th/^{230}Th ratios and 232Th fluxes moving from sites in the east to the west, both in seawater and in the sediment broadly in line with the expected trend from Saharan dust inputs (Figure 3).

5.3 ^{230}Th-normalised flux trends with depth

With the complete scavenging of all the ^{230}Th produced by in-situ decay of dissolved ^{234}U and no dissolution of sediment, the vertical mass fluxes at any given location should be the same, independent of water depth. However, the dissolution of carbonate material (De

Villiers, 2005) leads to a reduction in the preserved vertical mass flux with increasing water depth, a feature that is most obvious at water depths greater than 2000 m (Francois et al., 1990; Henderson and Anderson, 2003; Francois et al., 2004; Figure 4b).

A more surprising result was the increase in ^{232}Th fluxes with depth. Given the prevailing view that in remote parts of the ocean, dust addition at the surface is the dominant mechanism that delivers ^{232}Th to the seafloor, our observation of large increases in apparent ^{232}Th fluxes with water depth at all locations sampled in this study is unexpected. No clear trends in ^{232}Th flux with sample age are recognised, and the exclusion of ^{232}Th flux data from samples >~5 ka does not alter the overall trends of ^{232}Th flux with depth rendering an age bias unlikely (Figure S1). Leached ^{232}Th fluxes were also calculated to investigate whether the trend of increasing flux with depth extends to the adsorbed fraction of ^{232}Th. There is a significant increase in adsorbed flux with depth, but the smaller magnitude of this change, in comparison to total ^{232}Th fluxes, suggests that the adsorbed fraction is less affected by the processes that produce the apparent increases in total ^{232}Th flux (supplementary Figure S2). The proportion of ^{232}Th that is in the absorbed phase can be estimated from supplementary Figure S2. Applying the method outlined by Hsieh et al. (2011) to our seawater data indicates dissolved fluxes of ^{232}Th increasing by a factor of about 2 from shallow to deep (supplementary information). The elevated dissolved ^{232}Th fluxes at depth could imply an additional source of dissolved ^{232}Th at depth. For example, continued dissolution of dust settling through the water column, dissolution of re-suspended sediment from the seamount, or alternatively lateral advection of high ^{232}Th bearing waters from the distant continental margins (Roy-Barman, 2009; Hayes et al., 2013). However, the trend of increasing ^{232}Th flux pervades the adsorbed, dissolved and lattice bound pools of ^{232}Th, so a mechanism that can explain all of these observations is required.

Our observation of increasing ^{232}Th fluxes with depth is not unique. For example, increasing dissolved ^{232}Th fluxes with depth (from seawater) have previously been noted in the North Pacific (Hayes et al., 2013), and a previous study that reconstructed terrestrial fluxes into the tropical Atlantic using ^{230}Th-nomalisation also recorded increases in ^{232}Th and mass fluxes with depth at the Sierra Leone Rise and Ceara Rise (Francois and Bacon, 1991; Figure 4). The ^{232}Th fluxes at the Ceara Rise are elevated compared to the highest values presented in this study most likely explained by the proximity of the Ceara Rise to the South American continent and the Amazon River (Francois and Bacon, 1991). Francois and Bacon pointed towards the greatest increases in terrestrial fluxes with depth during the last deglacial period to the mid-Holocene. They suggested that variations in the exposure of continental shelves

during periods of low sea-level could have led to more continental material being delivered to the shelf edge from rivers such as the Amazon. They also suggested that resuspension of the slope sediments by western boundary currents could have led to increased fluxes of terrigenous material at depths >2800 m. Recent studies in the Atlantic do find some evidence for nepheloid layers at the ocean margins (Hayes et al., 2015a; Lam et al., 2015), but there is no clear evidence that they are consistent basin-wide features at the present day that could explain our observations.

If ^{232}Th fluxes accurately reflect continental inputs, they imply that greater than a factor of three times more continental material is supplied to the deep ocean compared to the shallow ocean at Carter Seamount, and over a factor of four at Vema. The increasing fluxes of ^{232}Th with depth cannot result from dust addition to the surface ocean and vertical sinking if our assumptions about ^{230}Th scavenging are correct. In order for ^{230}Th-normalised ^{232}Th fluxes to increase with depth, the ^{232}Th/^{230}Th ratio (from which fluxes are derived) must be higher at increasing depths than is expected from a linear increase of ^{230}Th and a constant vertical supply of ^{232}Th. In the following section we discuss three possible mechanisms that may lead to elevated ^{232}Th/^{230}Th ratios at depth and therefore explain the observed ^{232}Th flux trends: a) down slope transport of sediment with high ^{232}Th/^{230}Th or winnowing of fine sediments b) advection of ^{230}Th or ^{232}Th in the water column, c) dissolution of carbonate sediment and associated loss of ^{230}Th from the sediment.

5.3.1 Sediment transport

The redistribution of sediment of the seafloor is one of the drivers for the application of ^{230}Th normalisation to calculate vertical mass fluxes, as many sites are subject to significant lateral winnowing or focussing of sediment at the seafloor (Francois et al., 2004; Marcantonio et al., 2014). Sediment deposited at seamounts and other bathymetric features on the seafloor may be subject to down-slope redistribution driven by gravity (Stanley and Taylor, 1977). Indeed, the potential importance of internal tides for re-suspending sediment on seamounts with specific slope criticality (Peine et al., 2009) could provide a potential mechanism for the redistribution of sediment after deposition. In addition the presence of pronounced benthic nepheloid layers has been identified in parts of the Atlantic, highlighting the re-suspension and potential movement of fine sediments (McCave, 1986; Lam et al., 2015).

A mechanism that would increase the ratio of $^{232}Th/^{230}Th$ with depth (relative to a constant input of continental material at the surface and the expected increase in $^{230}Th_{xs}$ from reversible scavenging), is the down-slope transport of sediment with high $^{232}Th/^{230}Th$ from shallow depths. Erosion and advection of aged sediment would also contribute to high $^{232}Th/^{230}Th$ due to decay of initial $^{230}Th_{xs}$. Below 2000m, there is an approximately linear systematic increase in ^{232}Th flux seen at our sample sites, so the amount of addition of sediment with elevated $^{232}Th/^{230}Th$ would have to be a systematic process and at each seamount and across a large depth range. For this mechanism to be a viable explanation, it is required that the adsorbed ^{230}Th on the sediment that is transported down slope does not re-equilibrate with the surrounding water. Francois et al. (1990) modelled this process, concluding that downslope transport could lead to an over-estimate in ^{230}Th-normalised mass fluxes of ~10% at depth. However, other studies have concluded that focused sediment can indeed re-equilibrate with dissolved ^{230}Th at the water depth at which the sediment is re-deposited (Thomson et al., 1993; Thomson et al., 1999; Thomson et al., 2006). If re-equilibration does occur relatively rapidly (Bacon and Anderson, 1982; Thomson et al., 2006; Thomas et al., 2006), then a relatively fast mode of transport, such as a mass flow, would be required to cause the observed trends in ^{232}Th fluxes (i.e. faster than the re-equilibration timescale of Th). This interpretation relies on a continuous increase in ^{230}Th with depth in seawater.

A second transport mechanism may relate to the preferential movement of fine-grained sediment. Fine-grained sediments can be winnowed or focussed, depending on the sedimentary setting. It has been shown that fine-grained sediment accounts for a disproportionate amount of adsorbed $^{230}Th_{xs}$, and can be winnowed away, leading to potential biases in recorded ^{230}Th-normalised fluxes of sedimentary constituents in the coarse residual fraction (Kretschmer et al., 2010; McGee et al., 2010; Marcantonio et al., 2014). A consequence of such winnowing would be that the calculated ^{230}Th-normalised mass fluxes at our sample sites are in fact overestimated (Marcantonio et al, 2014). Recent studies argue that where terrestrial material is also dominantly in the fine fraction, fluxes of this component should not be biased by winnowing (Marcantonio et al., 2014; Costa and McManus, 2017), and so this mechanism for increasing apparent ^{230}Th-normalised ^{232}Th fluxes seems unlikely. Indeed, it has been shown that ^{232}Th is also enriched in the fine fraction of lithogenic sediments (Kretschmer et al., 2010; McGee et al., 2016). The potential for this mechanism to cause the observed changes in $^{232}Th/^{230}Th$ ratio would depend on one isotope being substantially more enriched than the other in the fine fraction.

It is not clear from the isotope data whether physical transport of sediment could cause the apparent increase in ^{232}Th flux with depth. The ^{230}Th-normalised detrital fluxes calculated using the residual mass of sediment, after removing carbonate, organic carbon and opal, also increase with depth (Figure 4d; Francois et al., 1990; Francois and Bacon, 1991). However, the magnitude of detrital flux increases is ~15-40% lower than the ^{232}Th flux increases. This result suggests that addition of ^{232}Th rich material (e.g. fine sediment associated with nepheloid layers) may be a viable mechanism to increase ^{232}Th/^{230}Th ratios at depth. The average concentration of ^{232}Th in the detrital material from the samples is 12.1 ± 0.9 μg g^{-1} (2 S.E.; supplementary data), lower than the 14 ± 1 μg g^{-1} value recommended by McGee et al. (2016) for dust flux reconstructions at locations distal to the source. The McGee et al. concentration is based on the <5 μm size fraction of dust, which typically has a higher concentration of ^{232}Th than the larger size fractions (e.g. Castillo et al., 2008). The presence of any lithogenic material >5 μm could lead to the lower concentration of ^{232}Th in our samples. This is plausible for at least some of our sample sites given that sediment traps close to the Carter site have recorded mean spherical equivalent grain sizes of up to 17 μm (Ratmeyer et al., 1999).

Alternatively, the higher than expected ^{232}Th fluxes at depth could point towards limitations in assumptions associated with ^{230}Th normalisation, rather than the systematics of lattice bound ^{232}Th, as discussed in the following sections.

5.2.2 Advection of ^{230}Th and ^{232}Th in the water column

The ^{230}Th-normalisation method relies on the assumption that the scavenged flux of ^{230}Th is equal to the production flux of ^{230}Th from the decay of ^{234}U in the water column (calculated using the uranium activity concentration and water depth). However, if ^{230}Th is advected away from the deep Atlantic (Moran et al., 2002; Hayes et al., 2015a), then this assumption may become compromised (Henderson et al., 1999). Advection of ^{230}Th has been demonstrated in the deep Atlantic by Moran et al. (2002). However, Deng et al. (2014) show that even relatively large changes in the concentration of dissolved ^{230}Th of up to 50% in the South Atlantic (imposed by enhanced bottom scavenging) lead to changes in the flux of ^{230}Th to the underlying sediment of less than 0.1%.

Far from other sources of lithogenic material such as rivers, the dissolved stock of ^{232}Th in the water column is generally thought to be controlled by the addition of windblown dust to the ocean (Hsieh et al., 2011; Singh et al., 2013; Hayes et al., 2013; Okubo et al., 2013; Deng et al., 2014; Hayes et al., 2015c; Lopez et al., 2015). However, other studies have highlighted the importance of riverine sources of continental material, and the possible

transport of slope sediments in nepheloid layers (Francois and Bacon, 1991). In places, elevated seawater ^{232}Th concentrations, in the North Atlantic for example, are thought to be due to the presence of specific water masses, implying that advection of ^{232}Th can control ^{232}Th profiles (Hsieh et al., 2011). Indeed, it has been suggested, through the use of modelling, that dissolved ^{232}Th in the water column can be influenced by the advection of water masses from continental margins (Roy-Barman, 2009). Our results from seawater samples indicate that windblown dust probably does have a control on the dissolved concentration of ^{232}Th. However, we cannot be sure that the entire inventory of ^{232}Th in the water column is derived entirely from the surface addition of dust and one-dimensional vertical sinking. Indeed, in an area subject to strong lateral advection such as the Atlantic ^{232}Th could be advected as has been shown for ^{230}Th (Moran et al., 2002). Unfortunately, the lack of clear systematic trends with depth in our dissolved ^{232}Th data make the identification of these processes difficult. With the advent of higher resolution data such as those from the GEOTRACES programme (e.g. Hayes et al., 2015a), the roles played by these processes may become clearer.

5.3.3 Carbonate dissolution and ^{230}Th loss

With post depositional carbonate dissolution (e.g. De Villiers, 2005), we expect the activity concentration of ^{230}Th in the sediment to increase with a preserved ^{230}Th-normalised mass flux decreasing accordingly if ^{230}Th is re-adsorbed entirely to the remaining sediment after dissolution (Henderson and Anderson, 2003; Francois et al., 2004). However, if some (or all) of the ^{230}Th associated with the dissolving sediment is not re-adsorbed to the remaining sediment, and there is minimal ^{232}Th in the carbonate, then dissolution may provide a mechanism that could change sedimentary ^{232}Th/^{230}Th ratios with depth. In this scenario the concentration of ^{230}Th will be reduced compared to complete re-adsorption, and the preserved ^{230}Th-normalised mass flux will be larger than the case where all of the ^{230}Th is retained. To test this idea we compare the extent of $CaCO_3$ dissolution (as also investigated by Francois et al., 1990) with the change in ^{232}Th and mass fluxes with depth. We use data from 2000 to > 4000m water depth at Carter, Knipovich and Vayda Seamounts which have the best resolved depth transects and clear trends in mass flux and ^{232}Th flux with depth.

We can calculate F, the proportion of the sediment remaining after dissolution at a depth > 4000 m, assuming that the sediment is a binary mixture of non-dissolving lithogenic sediment and $CaCO_3$ and using a reference carbonate concentration in the depth interval between ~2000 and 3000 m (supplementary information). This model assumes that changes in carbonate content are due to the dissolution of carbonate, rather than the addition of lithogenic material (i.e. that focussing is not occurring at the sites). F is 32%, 49% and 45%

515 at the three sites Carter, Knipovich and Vayda respectively. We can then compare these F
516 values to the change in preserved ^{230}Th-normalised mass flux over the same depth interval
517 (supplementary information). The proportion of ^{230}Th-normalised mass fluxes remaining at
518 depth for the same sites are 62%, 65% and 63% at the same three sites. The ^{230}Th-
519 normalised mass fluxes are larger than expected from the observed dissolution of carbonate,
520 implying that the $^{230}Th_{xs}$ concentration in the sediments is lower than expected if the only
521 factor in changing the $^{230}Th_{xs}$ concentration were the dissolution of sediment. From this
522 comparison 48%, 26% and 15% of the ^{230}Th must be lost from the sediment at Carter,
523 Knipovich and Vayda respectively in order to explain the discrepancy between the fraction of
524 sediment remaining and the fraction of ^{230}Th-normalised mass fluxes remaining at depth.
525
526 The same amount of ^{230}Th loss that may cause higher than predicted ^{230}Th-normalised mass
527 fluxes should also be able to explain the coincident increase in the apparent ^{232}Th flux
528 increase with depth. Assuming that there is no ^{232}Th in carbonate, the amount of ^{230}Th that
529 must be lost to explain the ^{232}Th data is 61%, 43%, 31% respectively. These values are up
530 to two times higher than the values calculated from the mass flux approach, but indicate that
531 loss of ^{230}Th during carbonate dissolution may be one of the processes responsible for the
532 apparent increase in ^{232}Th fluxes with depth.
533
534 The calculated deficit in ^{230}Th that is required to explain the observed trends in ^{230}Th-
535 normalised fluxes may be a result of advection, sediment redistribution or a combination of
536 all of the processes acting together, rather than only sediment dissolution. The size of the
537 ^{230}Th deficit must increase with depth in order to explain trends in ^{232}Th fluxes, so sediment
538 dissolution is a mechanism that could drive at least part of the trend, and is a process with a
539 well-defined depth dependence. In addition, if ^{230}Th is indeed lost from the sediment upon
540 carbonate dissolution and does not re-adsorb back to the sediment, there must exist some
541 mechanism which removes this ^{230}Th. Given previous observations in the Atlantic, lateral
542 advection of ^{230}Th seems a plausible mechanism (Moran et al., 2002; Marchal et al., 2007;
543 Hayes et al., 2015). A steady state scenario would require this laterally advected ^{230}Th to be
544 scavenged elsewhere, for example in areas with enhanced local scavenging such as
545 nepheloid layers or mid-ocean ridges (e.g. Hayes et al., 2015b).
546
547 5.4 The use of ^{230}Th-normalised ^{232}Th fluxes to estimate continental input
548 Despite the variation of apparent ^{232}Th fluxes with depth that we have identified, and the
549 uncertainties associated with such a variation, ^{230}Th-normalised ^{232}Th fluxes may still
550 represent a useful tool in determining continental fluxes to the sediment (Anderson et al.,
551 2016; Kienast et al., 2016). This is made clear when placed in the context of other

552 techniques that are available in order to estimate dust fluxes, such as models. These other
553 techniques can have uncertainties on the order of a factor of 10 (Mahowald et al., 2005) and
554 have not satisfactorily reproduced observational data for the modern day (Evan et al., 2014).
555 Calculated ^{232}Th fluxes for sediments at depths <1500 m are scattered and do not show a
556 recognisable trend with distance from the source of continental material (Figure 4c).
557 Therefore these samples cannot be considered to be accurately reproducing the trend of
558 modern dust input. Sediment samples at the greatest depths may have been subjected to
559 the greatest degree of the processes discussed above, such as carbonate dissolution. We
560 propose, therefore, that samples from the depth interval ~1500 -3000 m can give the best
561 estimate of representative ^{232}Th fluxes to the sediment in our study area (and therefore also
562 represent our best estimate of continental input), as summarised in Figure 6. Given the
563 processes affecting sedimentary ^{232}Th/^{230}Th from seasonal variations in the dust plume to
564 thorium advection, sediment redistribution and diagenesis, we would not expect a linear
565 trend of ^{232}Th fluxes from east to west. However, using this approach we do see an east to
566 west decrease in ^{232}Th flux of a factor of ~0.5. The average dissolved ^{232}Th flux
567 reconstructed from seawater reveals a similar change (a factor of ~0.7), although the
568 absolute ^{232}Th flux in the dissolved phase is approximately a factor of 4 lower (Figure 6).
569 This decrease in ^{232}Th flux is of the same order of magnitude to that presented by Anderson
570 et al., (2016) for a set of cores ~10^{o} to the north (averaging a factor of ~0.8 decrease from
571 east to west when excluding data that lie closer to the continent than our samples). Data
572 from previous studies show good agreement with the range of ^{232}Th fluxes calculated in this
573 study at SLR and the central tropical Atlantic (Figure 6; Francois and Bacon, 1991; core
574 VM20-234, Williams et al., 2016). The longitudinal transect of sedimentary ^{232}Th fluxes
575 presented by Anderson et al. (2016) are on average ~32% higher in the East and ~46%
576 lower values in the West than the 1500-3000 m fluxes of our transect. Differences in the
577 latitude of the transects may contribute to some of the disparity. At CR the values of ^{232}Th
578 flux are considerably elevated above those found at a similar longitude from this study
579 (Vema site), likely as a result of lithogenic sediment input to CR from the Amazon River
580 (Francois and Bacon, 1991; Figure 6).
581
582 5.5 Apparent fractional solubility of ^{232}Th
583 Estimates of ^{232}Th solubility represent a large uncertainty in calculating detrital fluxes from
584 seawater ^{232}Th/^{230}Th ratios (Hsieh et al., 2011; Anderson et al., 2016). Estimates of this
585 solubility may also be important in relation to the release of other trace metals from detrital
586 material in seawater (Hayes et al., 2015c; Anderson et al., 2016). Our seawater ^{232}Th/^{230}Th
587 ratios paired with sedimentary ratios from the nearest sample sites can be used to derive an
588 apparent fractional solubility of ^{232}Th from dust, with the caveat that if not all dissolved ^{232}Th

589 is derived from the dissolution of dust added at the surface, then the solubility will be
590 overestimated by a degree that is dependent on the amount of advected ^{232}Th (Figure 7).
591
592 This estimation can be made because the difference between the seawater $^{232}Th/^{230}Th$ ratio
593 and the sedimentary ratio is only a function of how much ^{232}Th is released from the dust to
594 the water, i.e. if half of the ^{232}Th were released, the seawater and sediment $^{232}Th/^{230}Th$ ratio
595 would differ by a factor of two (Equation 4).
596
597 Equation 4: Apparent fractional solubility = $[^{232}Th/^{230}Th]_{SW} / [^{232}Th/^{230}Th_{xs}]_{Sed}$
598
599 Our results indicate that the apparent fractional solubility of ^{232}Th from continental material is
600 not systematically dependent on depth at any of the sample locations (Figure 7). The
601 calculated solubilities range from 18 to 67 %, with an average solubility of 33%. Of the
602 solubilities calculated, 14 out of 17 values lie in the relatively narrow range 18-35% (Figure
603 7; supplementary information). These estimates are generally consistent with some of the
604 upper estimates of ^{232}Th solubility made by previous studies. Hayes et al., (2013) make
605 model-based estimates of ^{232}Th solubility up to 40%, although they prefer an estimate closer
606 to 20% based on the refractory nature of Th. Okubo et al., (2013) measure the solubility of
607 ^{232}Th from atmospherically deposited aerosol samples to be ~20% and Arraes-Mescoff et al.,
608 (2001) measure the percentage dissolution of ^{232}Th from particles to be up to ~13%. A
609 recent study from the North Atlantic estimates the likely range of thorium solubilities at
610 depths of 100 m to lie between 14-28% (Hayes et al., 2017), a range that agrees with the
611 majority of our estimates (Figure 7). The authors also calculate higher solubilities between
612 31-63% at depths up to 500 m, but conclude that these estimates may be influenced by
613 water masses bearing a ^{232}Th signature carried from elsewhere. These higher estimates still
614 lie within the solubility range estimated in this study.
615
616 It is possible that because seawater samples were collected close to the ocean floor that the
617 dissolution of any re-suspended sediments could lead to elevated ^{232}Th concentrations in the
618 seawater samples, and therefore bias the estimate of solubility, however the relatively
619 narrow range of solubilities from various locations and depths would argue against this
620 process being dominant. It is also possible, given the relatively large core-top ages of some
621 of our sediments, that the seawater-sediment comparison results in comparison of thorium
622 signals with different ages, and so the estimates of solubility could be dependent on changes
623 in ^{232}Th fluxes with time.
624

625 The average value of apparent solubility from this study of 29 ± 3% (2 s.e., n=15, excluding
626 the two outliers circled in Figure 7), could be used as a general estimate of ^{232}Th solubility for
627 studies that require such a value to extrapolate total ^{232}Th fluxes and detrital fluxes from
628 dissolved ^{232}Th fluxes (e.g. Hsieh et al., 2011; Hayes et al., 2013; Deng et al., 2014). This
629 value is slightly higher than the range suggested by Hayes et al. (2013) of 20 ± 5%, and may
630 be more appropriate as our study utilizes co-located samples to estimate solubility
631 (Anderson et al., 2016).
632
633 6. Conclusions
634 Both seawater and sedimentary ^{232}Th/^{230}Th ratios show a broad decreasing trend moving
635 west away from the African continent towards South America, consistent with expected
636 overall dust deposition patterns in the Tropical North Atlantic. However, the large depth
637 dependence of sedimentary ^{232}Th fluxes observed at all five of our sample locations
638 suggests an additional degree of complexity associated with the interpretation of ^{230}Th-
639 normalised ^{232}Th fluxes.
640
641 The mechanism that leads to increased ^{232}Th fluxes at depth remains uncertain, and may be
642 due to geochemical processes (such as the loss of ^{230}Th upon carbonate dissolution),
643 physical processes (e.g. advection by deep waters or sediment redistribution), or a
644 combination of processes. Further study of ^{232}Th fluxes with depth in seawater, particles and
645 sediment phases at other locations are required to further investigate these mechanisms.
646 The combined use of other geochemical proxies for lithogenic inputs which may not be
647 sensitive to the processes described above (such as ^{4}He/^{3}He) may help to disentangle some
648 of the possible mechanisms acting. Notwithstanding this depth dependence, we propose that
649 ^{232}Th fluxes measured in sediment in the depth interval between ~1500 -3000 m provide the
650 best estimate of representative ^{232}Th fluxes at our sample sites. By combining
651 measurements of ^{232}Th/^{230}Th in seawater and core-top sediments we have been able to
652 derive an apparent fractional solubility of ^{232}Th of 29 ± 3%, in reasonable agreement with the
653 upper end of existing estimates.
654
655 **Acknowledgements**
656 We acknowledge the science team and crew of JC094 for collecting and supplying sample
657 material. The authors would like to thank Carolyn Taylor for her laboratory assistance in
658 performing sediment leaching experiments and Chris Coath for his help in the Bristol Isotope
659 Group. We acknowledge funding from The European Research Council, a Marie Curie
660 Reintegration grant, the Leverhulme Trust and a Natural Environment Research Council
661 studentship.

662
663
664
665
666
667
668
669
670
671
672
673
674
675
676
677

References

Anderson R. F., Cheng H., Edwards R. L., Fleisher M. Q., Hayes C. T., Huang K.-F., Kadko D., Lam P. J., Landing W. M., Lao Y., Lu Y., Measures C. I., Moran S. B., Morton P. L., Ohnemus D. C., Robinson L. F. and Shelley R. U. (2016) How well can we quantify dust deposition to the ocean? Philos. Trans. R. Soc. A Math. Phys. Eng. Sci. 374.

Anderson R. F., Bacon M. P. and Brewer P. G. (1983) Removal of 230Th and 231Pa at ocean margins. *Earth Planet. Sci. Lett.* **66**, 73–90..

Anderson R. F., Fleisher M. Q. and Lao Y. (2006) Glacial-interglacial variability in the delivery of dust to the central equatorial Pacific Ocean. *Earth Planet. Sci. Lett.* **242**, 406–414.

Arraes-Mescoff R., Roy-Barman M., Coppola L., Souhaut M., Tachikawa K., Jeandel C., Sempéré R. and Yoro C. (2001) The behavior of Al, Mn, Ba, Sr, REE and Th isotopes during in vitro degradation of large marine particles. *Mar. Chem.* **73**, 1–19.

Auro M. E., Robinson L. F., Burke A., Bradtmiller L. I., Fleisher M. Q. and Anderson R. F. (2012) Improvements to 232-thorium, 230-thorium, and 231-protactinium analysis in seawater arising from GEOTRACES intercalibration. *Limnol. Oceanogr. Methods* **10**, 464–474.

Bacon M. P. and Anderson R. F. (1982) Distribution of thorium isotopes between dissolved and particulate forms in the deep sea. *J. Geophys. Res.* **87**, 2045.

Beaulieu S. E., Baker E. T. and German C. R. (2015) Where are the undiscovered hydrothermal vents on oceanic spreading ridges? *Deep Sea Res. Part II Top. Stud. Oceanogr.* 121, 202–212.

Broecker W. S., Kaufman A. and Trier R. M. (1973) The residence time of thorium in surface sea water and its implications regarding the rate of reactive pollutants. *Earth Planet. Sci. Lett.* **20**, 35–44.

Cakmur R. V, Miller R. L., Perlwitz J., Geogdzhayev I. V, Ginoux P., Koch D., Kohfeld K. E., Tegen I. and Zender C. S. (2006) Constraining the magnitude of the global dust cycle by minimizing the difference between a model and observations. *J. Geophys. Res. Atmos.* **111**.

Castillo S., Moreno T., Querol X., Alastuey A., Cuevas E., Herrmann L., Mounkaila M. and Gibbons W. (2008) Trace element variation in size-fractionated African desert dusts. *J. Arid Environ.* **72**, 1034–1045.

Costa K. and McManus J. (2017) Efficacy of 230Th normalization in sediments from the Juan de Fuca Ridge, northeast Pacific Ocean. *Geochim. Cosmochim. Acta* **197**, 215–225.

Chen T., Robinson L. F., Burke A., Southon J., Spooner P., Morris P. J. and Ng H. C. (2015) Synchronous centennial abrupt events in the ocean and atmosphere during the last deglaciation. Sci. 349, 1537–1541.

Cheng H., Edwards R. L., Shen C.-C., Polyak V. J., Asmerom Y., Woodhead J., Hellstrom J., Wang Y., Kong X., Spötl C., Wang X. and Jr. E. C. A. (2013) Improvements in 230Th dating, 230Th and 234U half-life values, and U–Th isotopic measurements by multi-collector inductively coupled plasma mass spectrometry. *Earth Planet. Sci. Lett.* **371–372**, 82–91.

Costa K. M., McManus J. F., Anderson R. F., Ren H., Sigman D. M., Winckler G., Fleisher M. Q., Marcantonio F. and Ravelo A. C. (2016) No iron fertilization in the equatorial Pacific Ocean during the last ice age. *Nature* **529**, 519–522.

De Villiers S. (2005) Foraminiferal shell-weight evidence for sedimentary calcite dissolution above the lysocline. *Deep. Res. Part I Oceanogr. Res. Pap.* **52**, 671–680.

Deng F., Thomas A. L., Rijkenberg M. J. A. and Henderson G. M. (2014) Controls on seawater 231Pa, 230Th and 232Th concentrations along the flow paths of deep waters in the Southwest Atlantic. *Earth Planet. Sci. Lett.* **390**, 93–102.

Eglinton T. I., Eglinton G., Dupont L., Sholkovitz E. R., Montluçon D. and Reddy C. M. (2002) Composition, age, and provenance of organic matter in NW African dust over the Atlantic Ocean. *Geochemistry, Geophys. Geosystems* **3**, 1–27.

Evan A. T., Flamant C., Fiedler S. and Doherty O. (2014) An analysis of aeolian dust in climate models. *Geophys. Res. Lett.* **41**, 5996–6001.

Francois R. and Bacon M. P. (1991) Variations in Terrigenous Input Into the Deep Equatorial Atlantic During the Past 24,000 Years. *Science* **251**, 1473–1476.

Francois R., Bacon M. P. and Suman D. O. (1990) Thorium 230 profiling in deep-sea sediments: High-resolution records of flux and dissolution of carbonate in the equatorial Atlantic during the last 24,000 years. Paleoceanography 5, 761–787.

Francois R., Frank M., van der Loeff M. M. and Bacon M. P. (2004) 230Th normalization: An essential tool for interpreting sedimentary fluxes during the late Quaternary. *Paleoceanography* **19**.

Goudie A. S. and Middleton N. J. (2001) Saharan dust storms: nature and consequences. *Earth-Science Rev.* **56**, 179–204.

Harrison S. P., Kohfeld K. E., Roelandt C. and Claquin T. (2001) The role of dust in climate changes today, at the last glacial maximum and in the future. *Earth-Science Rev.* **54**, 43–80.

Hayes C. T., Anderson R. F., Fleisher M. Q., Huang K.-F., Robinson L. F., Lu Y., Cheng H., Edwards R. L. and Moran S. B. (2015a) 230 Th and 231 Pa on GEOTRACES GA03, the US GEOTRACES North Atlantic transect, and implications for modern and paleoceanographic chemical fluxes. *Deep Sea Res. Part II Top. Stud. Oceanogr.* **116**, 29–41.

Hayes C. T., Anderson R. F., Fleisher M. Q., Serno S., Winckler G. and Gersonde R. (2013) Quantifying lithogenic inputs to the North Pacific Ocean using the long-lived thorium isotopes. *Earth Planet. Sci. Lett.* **383**, 16–25.

Hayes C. T., Anderson R. F., Fleisher M. Q., Vivancos S. M., Lam P. J., Ohnemus D. C., Huang K.-F., Robinson L. F., Lu Y., Cheng H., Edwards R. L. and Moran S. B. (2015b) Intensity of Th and Pa scavenging partitioned by particle chemistry in the North Atlantic Ocean. *Mar. Chem.* **170**, 49–60.

Hayes C. T., Fitzsimmons J. N., Boyle E. A., McGee D., Anderson R. F., Weisend R. and Morton P. L. (2015c) Thorium isotopes tracing the iron cycle at the Hawaii Ocean Time-series Station ALOHA. *Geochim. Cosmochim. Acta* **169**, 1–16.

Hayes C. T., Rosen J., McGee D. and Boyle E. A. (2017) Thorium distributions in high and low dust regions and the significance for iron supply. *Global Biogeochem. Cycles*.

Henderson G. M. and Anderson R. F. (2003) The U-series Toolbox for Paleoceanography. *Rev. Mineral. Geochemistry* **52** , 493–531.

Henderson G. M., Heinze C., Anderson R. F. and Winguth A. M. E. (1999) Global distribution of the 230Th flux to ocean sediments constrained by GCM modelling. *Deep Sea Res. Part I Oceanogr. Res. Pap.* **46**, 1861–1893

Hoffmann D. L., Prytulak J., Richards D. A., Elliott T., Coath C. D., Smart P. L. and Scholz D. (2007) Procedures for accurate U and Th isotope measurements by high precision MC-ICPMS. *Int. J. Mass Spectrom.* **264**, 97–109.

Holden N. E. (1990) Total half-lives for selected nuclides. *Pure Appl. Chem.* **62**, 941–958.

Hsieh Y. Te, Henderson G. M. and Thomas A. L. (2011) Combining seawater 232Th and 230Th concentrations to determine dust fluxes to the surface ocean. *Earth Planet. Sci. Lett.* **312**, 280–290.

Hydes D. J. (1983) Distribution of aluminium in waters of the North East Atlantic 25°N to 35°N. *Geochim. Cosmochim. Acta* **47**, 967–973.

Jacobel A. W., McManus J. F., Anderson R. F. and Winckler G. (2016) Large deglacial shifts of the Pacific Intertropical Convergence Zone. *Nat Commun* **7**.

Jickells T. D., An Z. S., Andersen K. K., Baker A. R., Bergametti G., Brooks N., Cao J. J., Boyd P. W., Duce R. A., Hunter K. A., Kawahata H., Kubilay N., laRoche J., Liss P. S., Mahowald N., Prospero J. M., Ridgwell A. J., Tegen I. and Torres R. (2005) Global Iron Connections Between Desert Dust, Ocean Biogeochemistry, and Climate. *Sci*. **308**, 67–71.

Kienast S. S., Winckler G., Lippold J., Albani S. and Mahowald N. M. (2016) Tracing dust input to the global ocean using thorium isotopes in marine sediments: ThoroMap. Global Biogeochem. Cycles 30, 1526–1541.

Kohfeld K. E. and Harrison S. P. (2001) DIRTMAP: the geological record of dust. *Earth-Science Rev*. **54**, 81–114.

Kretschmer S., Geibert W., van der Loeff M. M. R. and Mollenhauer G. (2010) Grain size effects on 230Thxs inventories in opal-rich and carbonate-rich marine sediments. *Earth Planet*. *Sci*. *Lett*. **294**, 131–142.

Lawrence C. R. and Neff J. C. (2009) The contemporary physical and chemical flux of aeolian dust: A synthesis of direct measurements of dust deposition. *Chem*. *Geol*. **267**, 46–63.

Lam P. J., Ohnemus D. C. and Auro M. E. (2015) Size-fractionated major particle composition and concentrations from the US GEOTRACES north Atlantic zonal transect. *Deep Sea Res*. *Part II Top*. *Stud*. *Oceanogr*. **116**, 303–320.

Lam P. J., Robinson L. F., Blusztajn J., Li C., Cook M. S., McManus J. F. and Keigwin L. D. (2013) Transient stratification as the cause of the North Pacific productivity spike during deglaciation. *Nat*. *Geosci* **6**, 622–626.

Lerner P., Marchal O., Lam P. J., Anderson R. F., Buesseler K., Charette M. A., Edwards R. L., Hayes C. T., Huang K.-F., Lu Y., Robinson L. F. and Solow A. (2016) Testing models of thorium and particle cycling in the ocean using data from station GT11-22 of the U.S. GEOTRACES North Atlantic section. *Deep Sea Res*. *Part I Oceanogr*. *Res*. *Pap*. **113**, 57–79.

Lopez G. I., Marcantonio F., Lyle M. and Lynch-Stieglitz J. (2015) Dissolved and particulate 230Th–232Th in the Central Equatorial Pacific Ocean: Evidence for far-field transport of the East Pacific Rise hydrothermal plume. *Earth Planet*. *Sci*. *Lett*. **431**, 87–95.

Maher B. A., Prospero J. M., Mackie D., Gaiero D., Hesse P. P. and Balkanski Y. (2010) Global connections between aeolian dust, climate and ocean biogeochemistry at the present day and at the last glacial maximum. *Earth-Science Rev*. **99**, 61–97.

Mahowald N. M., Baker A. R., Bergametti G., Brooks N., Duce R. A., Jickells T. D., Kubilay N., Prospero J. M. and Tegen I. (2005) Atmospheric global dust cycle and iron inputs to the ocean. *Global Biogeochem*. *Cycles* **19**.

Marcantonio F., Lyle M. and Ibrahim R. (2014) Particle sorting during sediment redistribution processes and the effect on 230Th-normalized mass accumulation rates. *Geophys*. *Res*. *Lett*. **41**, 5547–5554.

Marchal O., François R. and Scholten J. (2007) Contribution of 230Th measurements to the estimation of the abyssal circulation. *Deep Sea Res*. *Part I Oceanogr*. *Res*. *Pap*. **54**, 557–585.

McCave I. N. (1986) Local and global aspects of the bottom nepheloid layers in the world ocean. *Netherlands J*. *Sea Res*. **20**, 167–181.

McGee D., deMenocal P. B., Winckler G., Stuut J. B. W. and Bradtmiller L. I. (2013) The magnitude, timing and abruptness of changes in North African dust deposition over the last 20,000 yr. Earth Planet. Sci. Lett. 371–372, 163–176

McGee D., Marcantonio F. and Lynch-Stieglitz J. (2007) Deglacial changes in dust flux in the eastern equatorial Pacific. *Earth Planet. Sci. Lett.* **257**, 215–230.

McGee D., Marcantonio F., McManus J. F. and Winckler G. (2010) The response of excess 230Th and extraterrestrial 3He to sediment redistribution at the Blake Ridge, western North Atlantic. *Earth Planet. Sci. Lett.* **299**, 138–149.

McGee D., Winckler G., Borunda A., Serno S., Anderson R. F., Recasens C., Bory A., Gaiero D., Jaccard S. L., Kaplan M., McManus J. F., Revel M. and Sun Y. (2016) Tracking eolian dust with helium and thorium: Impacts of grain size and provenance. *Geochim. Cosmochim. Acta* **175**.

Measures C. I., Landing W. M., Brown M. T. and Buck C. S. (2008) High-resolution Al and Fe data from the Atlantic Ocean CLIVAR-CO2 Repeat Hydrography A16N transect: Extensive linkages between atmospheric dust and upper ocean geochemistry. *Global Biogeochem. Cycles* **22**.

Moran S. B., Shen C. C., Edmonds H. N., Weinstein S. E., Smith J. N. and Edwards R. L. (2002) Dissolved and particulate 231Pa and 230Th in the Atlantic Ocean: Constraints on intermediate/deep water age, boundary scavenging, and 231Pa/230Th fractionation. *Earth Planet. Sci. Lett.* **203**, 999–1014.

Mortlock R. A. and Froelich P. N. (1989) A simple method for the rapid determination of biogenic opal in pelagic marine sediments. *Deep Sea Res. Part A. Oceanogr. Res. Pap.* **36**, 1415–1426.

Niedermeier N., Held A., Müller T., Heinold B., Schepanski K., Tegen I., Kandler K., Ebert M., Weinbruch S., Read K., Lee J., Fomba K. W., Müller K., Herrmann H. and Wiedensohler A. (2014) Mass deposition fluxes of Saharan mineral dust to the tropical northeast Atlantic Ocean: an intercomparison of methods. *Atmos. Chem. Phys.* **14**, 2245–2266.

Okubo A., Obata H., Gamo T. and Yamada M. (2012) 230Th and 232Th distributions in mid-latitudes of the North Pacific Ocean: Effect of bottom scavenging. *Earth Planet. Sci. Lett.* **339–340**, 139–150.

Peine F., Turnewitsch R., Mohn C., Reichelt T., Springer B. and Kaufmann M. (2009) The importance of tides for sediment dynamics in the deep sea—evidence from the particulate-matter tracer 234 Th in deep-sea environments with different tidal forcing. *Deep Sea Res. Part I Oceanogr. Res. Pap.* **56**, 1182–1202.

Pourmand A., Marcantonio F. and Schulz H. (2004) Variations in productivity and eolian fluxes in the northeastern Arabian Sea during the past 110 ka. *Earth Planet. Sci. Lett.* **221**, 39–54.

Ratmeyer V., Fischer G. and Wefer G. (1999) Lithogenic particle fluxes and grain size distributions in the deep ocean off northwest Africa: Implications for seasonal changes of aeolian dust input and downward transport. *Deep Sea Res. Part I Oceanogr. Res. Pap.* **46**, 1289–1337.Ridley D. A., Heald C. L. and Ford B. (2012) North African dust export and deposition: A satellite and model perspective. *J. Geophys. Res. Atmos.* **117**.

Robinson L. F. (2014) RRS James Cook Cruise JC094, October 13–November 30 2013, Tenerife-Trinidad. TROPICS, Tracing Oceanic Processes using Corals and Sediments. Reconstructing abrupt Changes in Chemistry and Circulation of the Equatorial Atlantic Ocean. *Available at: http://epic.awi.de/35605/*

Robinson L. F., Belshaw N. S. and Henderson G. M. (2004) U and Th concentrations and isotope ratios in modern carbonates and waters from the Bahamas. *Geochim. Cosmochim. Acta* **68**, 1777–1789.

Robinson L. F., Noble T. L. and McManus J. F. (2008) Measurement of adsorbed and total 232Th/230Th ratios from marine sediments. *Chem. Geol.* **252**, 169–179.

Roy-Barman M. (2009) Modelling the effect of boundary scavenging on Thorium and Protactinium profiles in the ocean. *Biogeosciences* **6**, 3091–3107.

Serno S., Winckler G., Anderson R. F., Hayes C. T., McGee D., Machalett B., Ren H., Straub S. M., Gersonde R. and Haug G. H. (2014) Eolian dust input to the Subarctic North Pacific. *Earth Planet. Sci. Lett.* **387**, 252–263.

Singh A. K., Marcantonio F. and Lyle M. (2013) Water column 230 Th systematics in the eastern equatorial Pacific Ocean and implications for sediment focusing. *Earth Planet. Sci. Lett.* **362**, 294–304.

Stanley D. J. and Taylor P. T. (1977) Sediment transport down a seamount flank by a combined current and gravity process. *Mar. Geol.* **23**, 77–88.

Taylor S. R. and McLennan S. . (1985) The continental crust: Its composition and evolution. *McClennan, Blackwell Sci. Publ.* **21**, 85–86.

Thomson J., Colley S., Anderson R., Cook G. T., MacKenzie A. B. and Harkness D. D. (1993) Holocene sediment fluxes in the northeast Atlantic from 230Thexcess and radiocarbon measurements. *Paleoceanography* **8**, 631–650.

Thomson J., Green D. R. H., van Calsteren P., Richter T. O. and van Weering T. C. E. (2006) Holocene sediment deposition on a NE Atlantic transect including Feni Drift quantified by radiocarbon and 230Thexcess methods. *Earth Planet. Sci. Lett.* **242**, 170–185.

Thomson J., Nixon S., Summerhayes C. P., Schönfeld J., Zahn R. and Grootes P. (1999) Implications for sedimentation changes on the Iberian margin over the last two glacial/interglacial transitions from (230Thexcess)0 systematics. *Earth Planet. Sci. Lett.* **165**, 255–270.

Wang X., Murtugudde R., Hackert E. and Marañón E. (2013) Phytoplankton carbon and chlorophyll distributions in the equatorial Pacific and Atlantic: a basin-scale comparative study. *J. Mar. Syst.* **109**, 138–148.

Williams R. H., McGee D., Kinsley C. W., Ridley D. A., Hu S., Fedorov A., Tal I., Murray R. W. and deMenocal P. B. (2016) Glacial to Holocene changes in trans-Atlantic Saharan dust transport and dust-climate feedbacks. *Sci. Adv. 2*.

Winckler G., Anderson R. F., Fleisher M. Q., McGee D. and Mahowald N. (2008) Covariant glacial-interglacial dust fluxes in the equatorial Pacific and Antarctica. *Science* **320**, 93–*96*.

Figure1

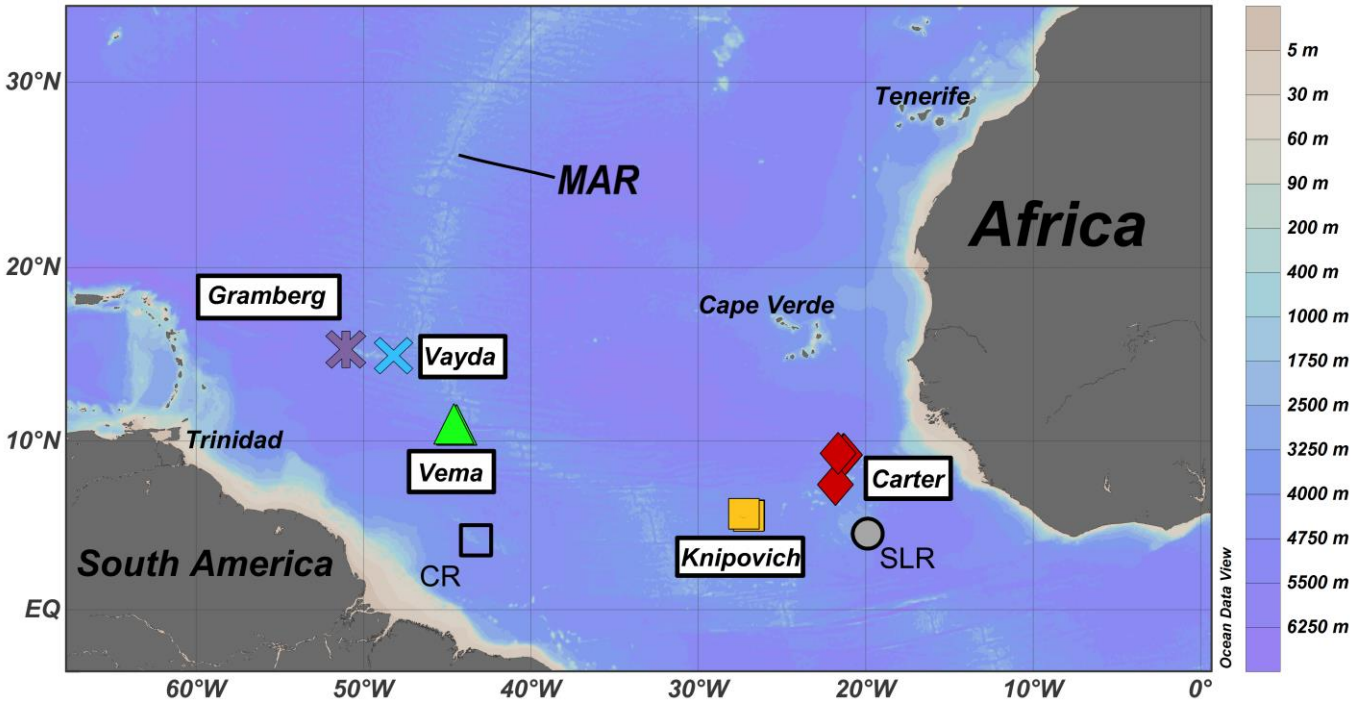
30°N
20°N
10°N
EQ
60°W
50°W
40°W
30°W
20°W
10°W
0°
MAR
Africa
Tenerife
Cape Verde
Gramberg
Vayda
Vema
Trinidad
South America
CR
Knipovich
Carter
SLR
5 m
30 m
60 m
90 m
200 m
400 m
1000 m
1750 m
2500 m
3250 m
4000 m
4750 m
5500 m
6250 m
Ocean Data View

Figure1 caption

Figure 1. Map of JC094 sites where the samples of sediment and seawater for this study were collected. The sites are named based on their proximity to bathymetric features. The start and end points of the cruise are indicated (Tenerife and Trinidad respectively) as well as the Mid-Atlantic ridge (MAR). CR = Ceara rise, SLR= Sierra Leone rise (Francois et al., 1990).

Figure2

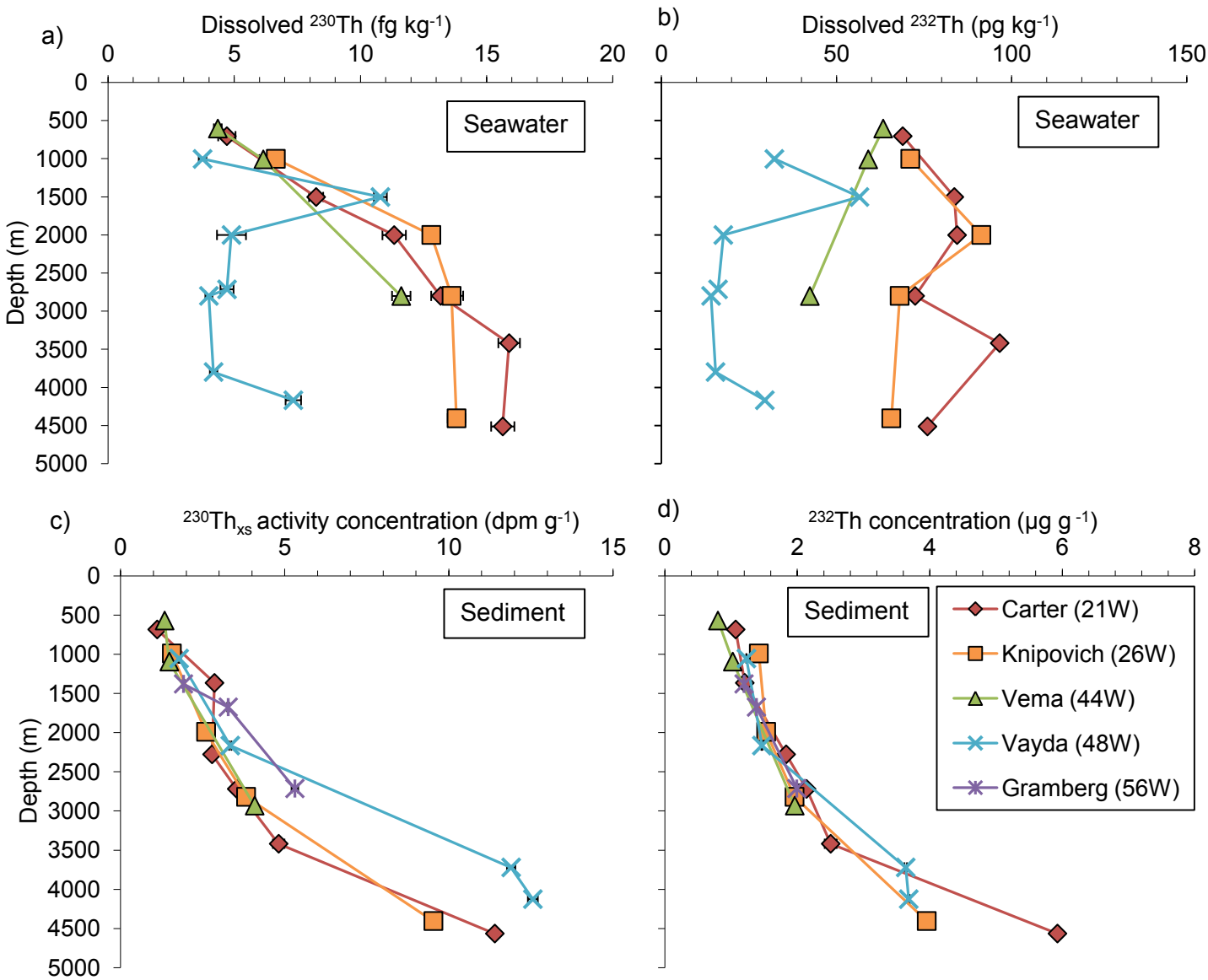
a)
Dissolved 230Th (fg kg-1)
0
5
10
15
20
Seawater
Depth (m)
0
500
1000
1500
2000
2500
3000
3500
4000
4500
5000
b)
Dissolved 232Th (pg kg-1)
0
50
100
150
Seawater
c)
230Thxs activity concentration (dpm g-1)
0
5
10
15
Sediment
d)
232Th concentration (µg g -1)
0
2
4
6
8
Sediment
Carter (21W)
Knipovich (26W)
Vema (44W)
Vayda (48W)
Gramberg (56W)

Figure2 caption

Figure 2. Concentrations of a) ^{230}Th and b) ^{232}Th in filtered seawater samples and concentrations of c) $^{230}Th_{xs}$ and d) ^{232}Th in sediment core-tops. Where error bars are not visible they are smaller than the symbols used. The approximate longitude of each sampling locations is given in the key.

Figure3

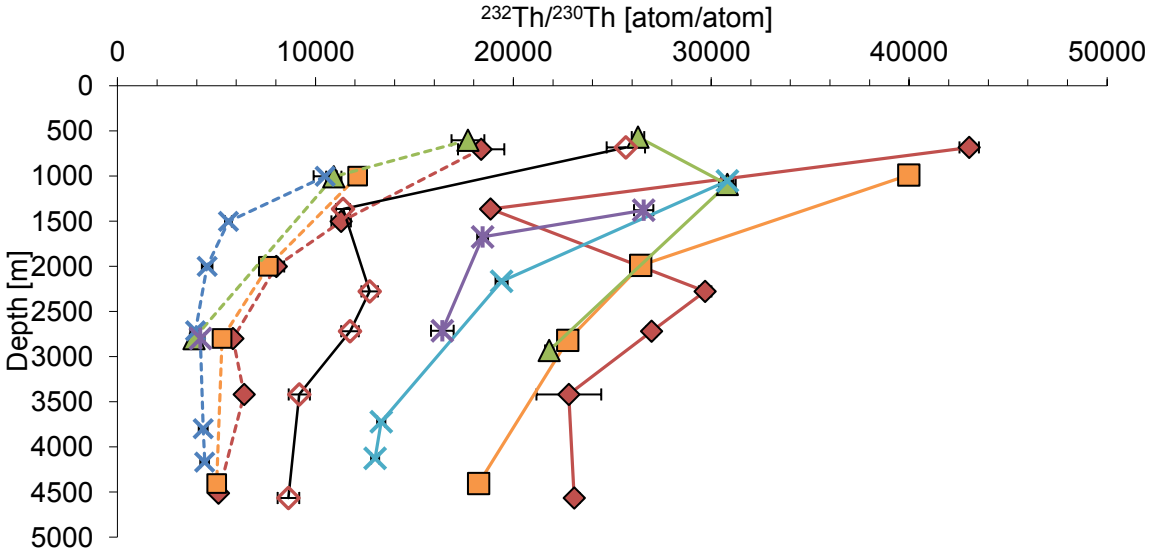
232Th/230Th [atom/atom]
0
10000
20000
30000
40000
50000
Depth [m]
0
500
1000
1500
2000
2500
3000
3500
4000
4500
5000

Figure3 caption

Figure 3. Atomic ratios of $^{232}Th/^{230}Th_{xs}$ in seawater (dashed lines) and core-top sediment samples (solid lines) with depth. Ratios derived from leaching of Carter sediments are presented as hollow diamonds. Error bars represent 2 standard deviations from the mean, reflecting analytical uncertainty.

Figure4

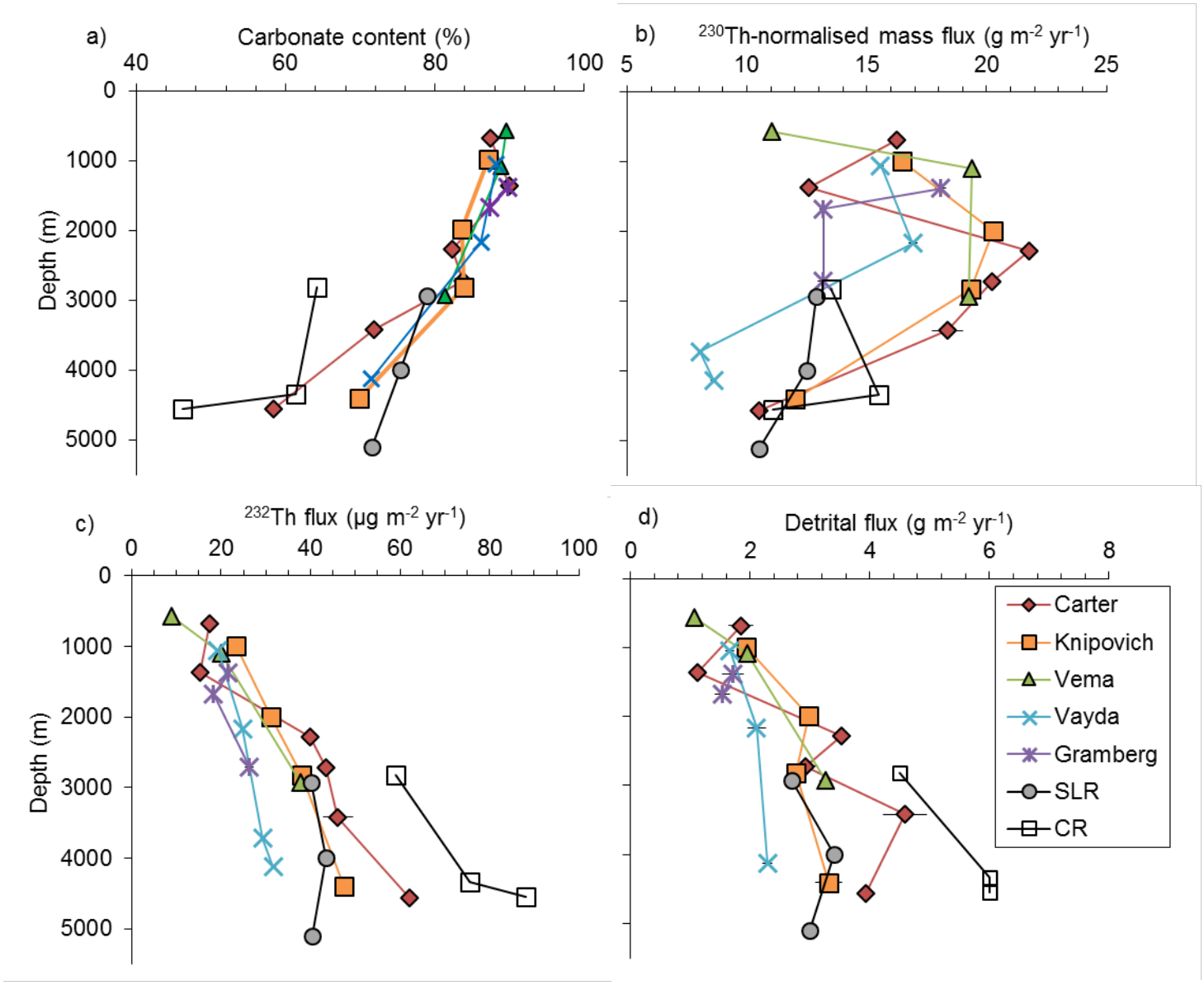
a)
Carbonate content (%)
40
60
80
100
0
1000
2000
3000
4000
5000
Depth (m)
b)
230Th-normalised mass flux (g m-2 yr-1)
5
10
15
20
25
c)
232Th flux (µg m-2 yr-1)
0
20
40
60
80
100
Depth (m)
d)
Detrital flux (g m-2 yr-1)
0
2
4
6
8
Carter
Knipovich
Vema
Vayda
Gramberg
SLR
CR

Figure4 caption

Figure 4. a) Carbonate content, b) ^{230}Th-normalised mass fluxes c) ^{230}Th-normalised ^{232}Th fluxes d) ^{230}Th-normalised detrital fluxes. Error bars give 2 standard deviations from the mean, and represent the analytical uncertainty. SLR (= Sierra Leone rise) and CR (= Ceara rise) are data from Francois et al. (1990), from samples at the shallowest possible core depths (<3.5 cm from the core-top) all with model ages of <2 kyr (Francois et al., 1990).

Figure5 revised

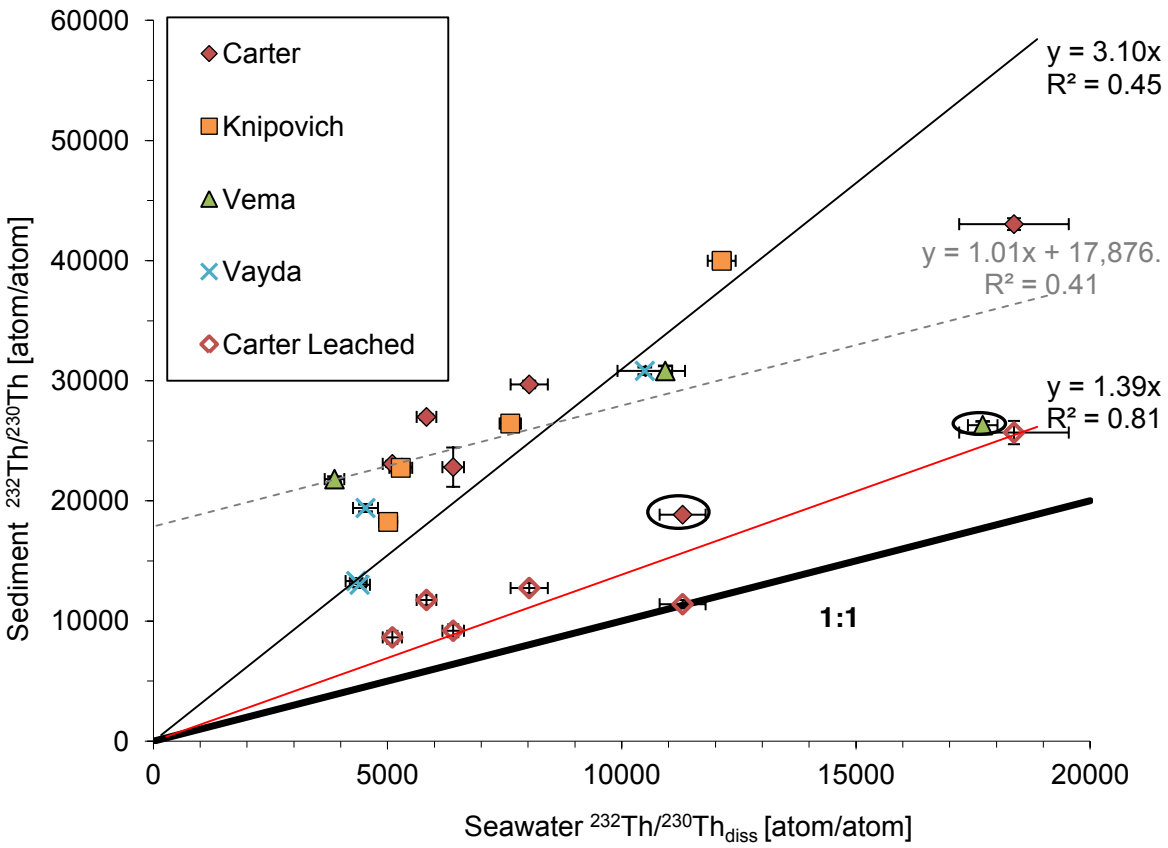

Figure5 caption revised

Figure 5. Comparison of $^{232}Th/^{230}Th_{xs}$ in sediment core-tops and seawater samples (solid symbols). A linear regression for sediment and seawater data is shown by the thin black line, with the two circled data points not included in the regression (inclusion of these data gives R^2 =0.41, shown by the grey dashed regression line). Hollow red diamonds indicate leached core-top sediments and seawater $^{232}Th/^{230}Th$ from Carter Seamount; a linear regression is shown by the red line. All error bars represent 2 standard deviations from the mean, reflecting the analytical uncertainty.

Figure6

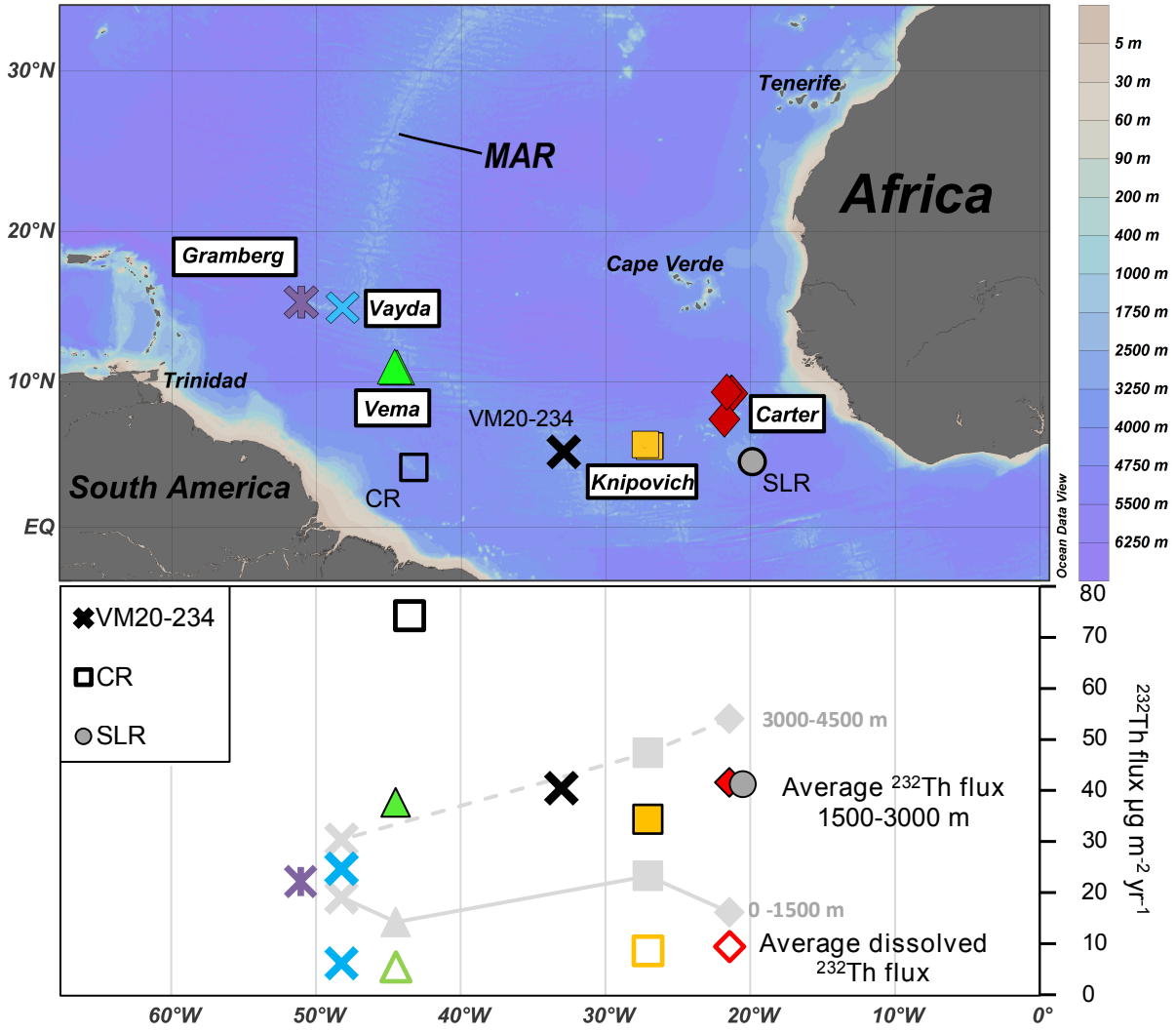
30°N
20°N
10°N
EQ
MAR
Tenerife
Africa
Cape Verde
Gramberg
Vayda
Trinidad
Vema
VM20-234
Carter
Knipovich
SLR
CR
South America
Ocean Data View
5 m
30 m
60 m
90 m
200 m
400 m
1000 m
1750 m
2500 m
3250 m
4000 m
4750 m
5500 m
6250 m
VM20-234
CR
SLR
3000-4500 m
Average 232Th flux
1500-3000 m
0 -1500 m
Average dissolved
232Th flux
232Th flux µg m-2 yr-1
80
70
60
50
40
30
20
10
0
60°W
50°W
40°W
30°W
20°W
10°W
0°

Figure6 caption

Figure 6. Upper panel shows a map of sample sites whilst the lower panel shows total ^{230}Th-normalised ^{232}Th fluxes and dissolved ^{232}Th fluxes. The grey symbols show sedimentary ^{230}Th-normalised ^{232}Th fluxes at each site for the specified depth interval. The solid colour symbols represent sedimentary ^{232}Th fluxes over the depth interval 1500-3000 m, as a best estimate of representative ^{232}Th fluxes for each site. The hollow colour symbols show the average dissolved ^{232}Th fluxes at each location calculated from seawater. CR and SLR show average core-top ^{232}Th fluxes of the three cores at each location (Francois and Bacon, 1991). The core-top ^{232}Th flux from VM20-234 is taken from Williams et al. (2016).

Figure7

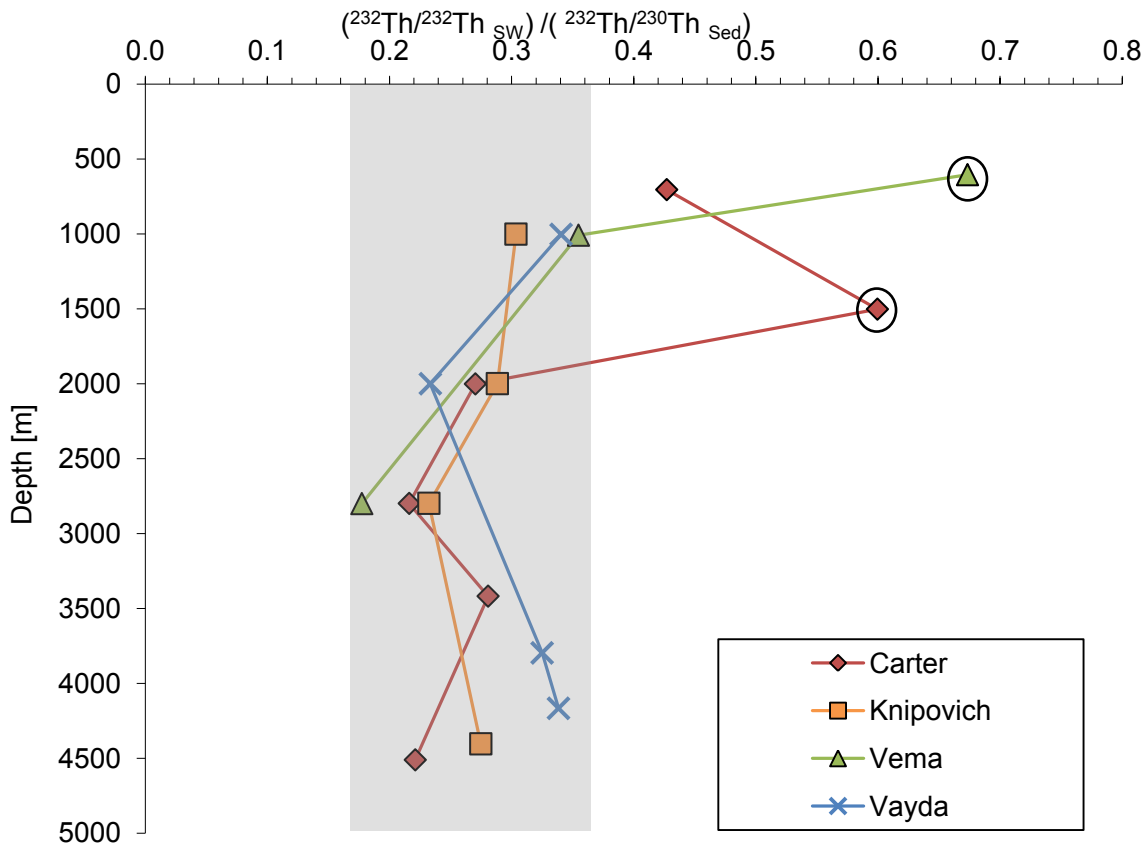
(232Th/232Th SW) /(232Th/230Th Sed)
0.0
0.1
0.2
0.3
0.4
0.5
0.6
0.7
0.8
Depth [m]
0
500
1000
1500
2000
2500
3000
3500
4000
4500
5000
Carter
Knipovich
Vema
Vayda

Figure7 caption

Figure 7. Apparent fractional solubility of ^{232}Th from lithogenic material based on the ratio of seawater and core-top $^{232}Th/^{230}Th_{xs}$ ratios. All but three samples lie within a relatively narrow range (18-35 %) highlighted in grey. The two circled data points are the two points that are excluded from the regression in Figure 5.

supplementary Figure S1

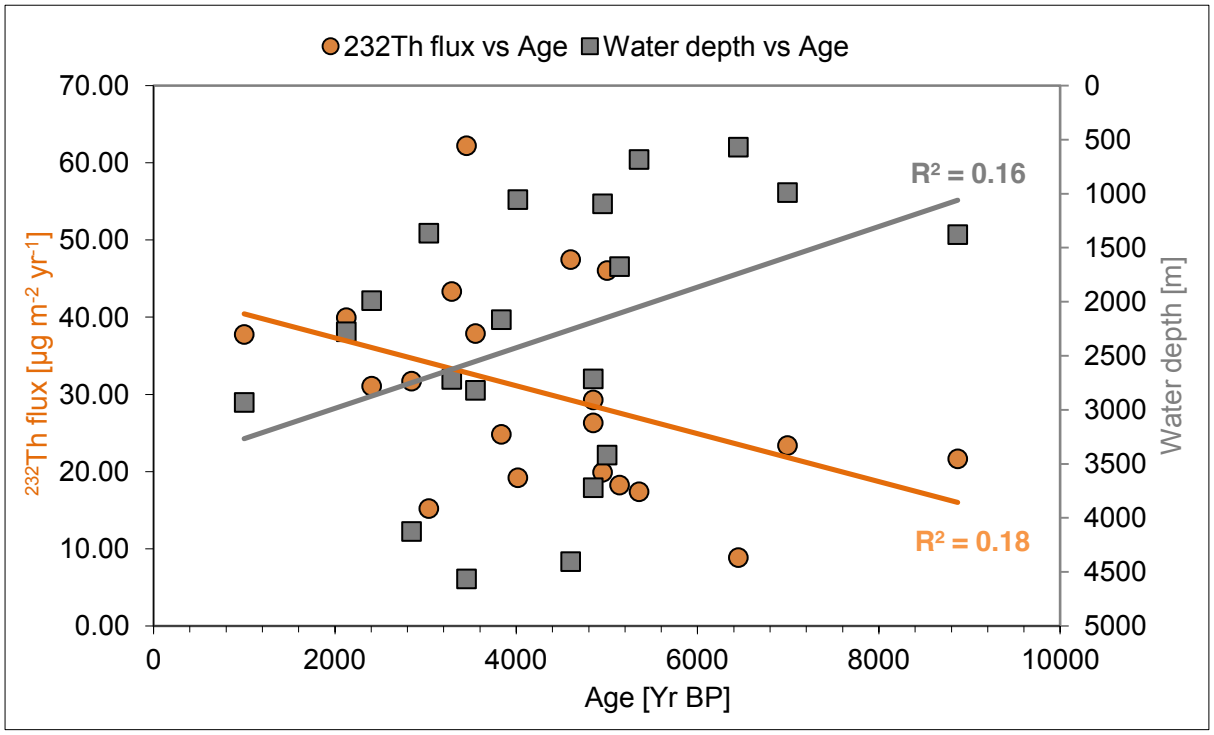

supplementary Figure S1 caption

Figure S1. Core-top ages plotted against ^{232}Th flux (orange circles) and water depth (grey squares).

supplementary Figure S2

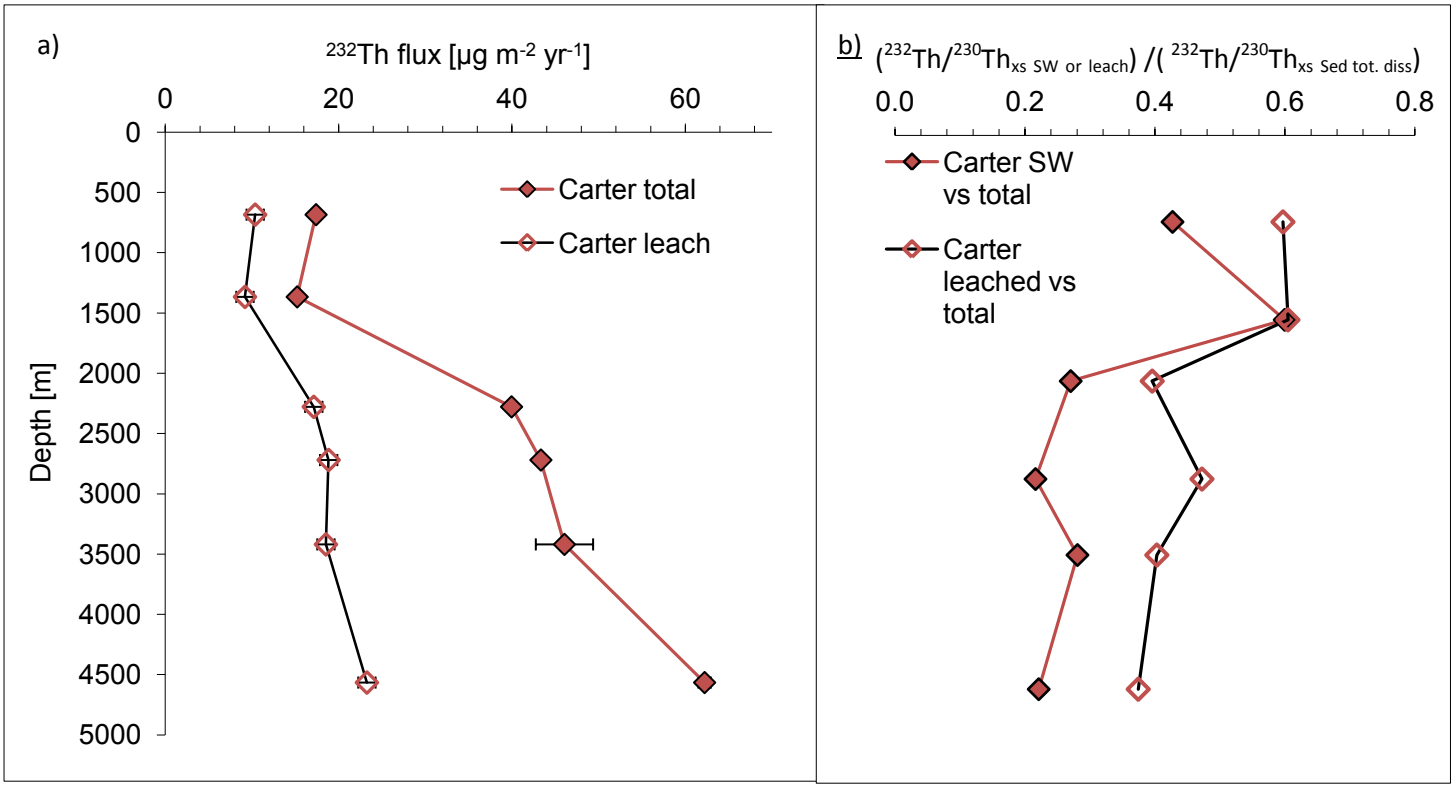

supplementary Figure S2 caption

Figure S2. a) Leached (adsorbed) and total ^{232}Th fluxes from the Carter site. b) Comparisons of $^{232}Th/^{230}Th_{xs}$ at Carter between seawater and total sediment dissolutions (solid diamonds) and between sediment leachates and total sediment dissolutions (hollow diamonds).

supplementary information

Click here to download Electronic Annex: 232Th_230Th GHR et al. Supplement_Revised.docx

supplementary data

Click here to download Electronic Annex: 232Th_230Th GHR et al. supplementary_data_Revised.xlsx

Equation1 as PDF

Click here to download Source or Other Companion File: 232Th_230Th GHR et al. Equation 1.pdf

Equation2 as PDF

Click here to download Source or Other Companion File: 232Th_230Th GHR et al. Equation 2.pdf

Equation3 as PDF

Click here to download Source or Other Companion File: 232Th_230Th GHR et al. Equation 3.pdf

Equation 4 revised

Click here to download Source or Other Companion File: Equation 4 Revised.pdf

Supplement Equation1 as PDF

Click here to download Source or Other Companion File: 232Th_230Th GHR et al. Equation S1.pdf

Supplement Equation2 as PDF

Click here to download Source or Other Companion File: 232Th_230Th GHR et al. Equation S2.pdf

Supplement Equation3 as PDF

Click here to download Source or Other Companion File: 232Th_230Th GHR et al. Equation S3.pdf

Supplement Equation4 as PDF

Click here to download Source or Other Companion File: 232Th_230Th GHR et al. Equation S4.pdf

Supplement Equation5 as PDF

Click here to download Source or Other Companion File: 232Th_230Th GHR et al. Equation S5.pdf